

## Numerical Methods for the Analysis of Dynamics and Synchronization of Stochastic Nonlinear Systems

How-Foo Chen and Jia-Ming Liu

**Summary.** The most important numerical tools needed in the analysis of chaotic systems performing chaos synchronization and chaotic communications are discussed in this chapter. Basic concepts, theoretical framework, and computer algorithms are reviewed. The subjects covered include the concepts and numerical simulations of stochastic nonlinear systems, the complexity of a chaotic attractor measured by Lyapunov exponents and correlation dimension, the robustness of synchronization measured by the transverse Lyapunov exponents in parameter-matched systems and parameter-mismatched systems, the quality of synchronization measured by the correlation coefficient and the synchronization error, and the treatment of channel noise for quantifying the performance of a chaotic communication system. For a dynamical system described by stochastic differential equations, the integral of a stochastic term is very different from that of a deterministic term. The difference and connection between two different stochastic integrals in the Ito and Stratonovich senses, respectively, are discussed. Numerical algorithms for the simulation of stochastic differential equations are developed. Two quantitative measures, namely, the Lyapunov exponents and the correlation dimension, for a chaotic attractor are discussed. Numerical methods for calculating these parameters are outlined. The robustness of synchronization is measured by the transverse Lyapunov exponents. Because perfect parameter matching between a transmitter and a receiver is generally not possible in a real system, a new concept of measuring the robustness of synchronization by comparing the unperturbed and perturbed receiver attractors is introduced for a system with parameter mismatch. For the examination of the quality of synchronization, the correlation coefficient and the synchronization error obtained by comparing the transmitter and the receiver outputs are used. The performance of a communication system is commonly measured by the bit-error rate as a function of signal-to-noise ratio. In addition to the noise in the transmitter and the receiver, the noise of the communication channel has to be considered in evaluating the bit-error rate and signal-to-noise ratio of the system. An approach to integrating the linear and non-linear effects of the channel noise into the system consistently is addressed. Optically injected single-mode semiconductor lasers are used as examples to demonstrate the use of these numerical tools.

## 9.1 Introduction

In developing a nonlinear dynamical system for chaos synchronization and chaotic communication, several important issues ranging from basic dynamical characteristics to system performances have to be studied. Besides experimental measurements and characterization, various numerical tools are generally needed for a thorough study of the system. Numerical simulation is usually a necessary approach to gaining a complete picture of various dynamical characteristics of a nonlinear system and predicting the dynamics of the system under certain operating conditions. Many parameters and operating conditions, although not easily controllable precisely in experiments, can be precisely prescribed in numerical simulations. Even in the experimental approach, it is also very important to use appropriate numerical methods to analyze the experiment data for a variety of purposes, such as the verification of the chaotic states, the analysis of the complexity of the observed chaos, the qualification of the achieved chaos synchronization, and the characterization of the system performance. The required numerical methods for these studies cover several aspects, including the nonlinear dynamics of a chaotic oscillator generating a chaotic output, the characteristics of the chaotic output, the feasibility of chaos synchronization for a proposed system, the robustness of synchronization, the quality of synchronization, and the performance of the system.

Any physical system always contains some intrinsic noise. Noise in a nonlinear dynamical system is not simply additive to the system dynamics but is an integral part of the dynamics. The dynamical state of a nonlinear system can often vary with the level of the noise in the system. When considering a communication system in reality, the effect of noise on many system performance indicators, such as the bit-error rate (BER), is a key issue that needs to be addressed. For a communication system that utilizes nonlinear dynamics, the effect of noise on the system performance can neither be fully understood nor correctly quantified without considering the nonlinear interactions between noise and system dynamics. Both intrinsic noise of the nonlinear devices and noise of the communication channel have to be considered. Because noise is random and nondeterministic, the Riemann–Stieltjes integrals for solving deterministic differential equations cannot be used for the numerical analysis and simulation of a noisy nonlinear system that is described by differential equations containing stochastic noise terms. Thus, the numerical methods for the analysis and simulation of the dynamics of a stochastic nonlinear system are nontrivial and have to be carefully formulated. In Section 9.2, the general concepts of a stochastic differential equation and its correct integral are first discussed, followed by the introduction of proper numerical algorithms for implementing the analysis and simulation of a system described by stochastic differential equations. The numerical method for the integration of channel noise in a communication system is discussed in Section 9.5.

Because a chaotic waveform generated by a transmitter is used in a chaotic communication system as the message carrier, the verification of its chaotic nature and the characterization of its complexity are both needed in this application. Various numerical methods for the analysis of chaos in the time domain, the frequency domain, or the phase space have been developed. In the time domain, the Lyapunov exponents can be calculated for a chaotic state to quantify the sensitivity of the state to the initial conditions. These parameters indicate the predictability, or rather the unpredictability, of the chaotic trace evolving in time. In the frequency domain, a chaotic waveform is characterized by a broadband spectrum that can be found by taking the Fourier transform of its time series. In the phase space, a chaotic state is characterized by a strange attractor of a fractal dimension. Several different definitions of chaotic attractor dimension are used to measure the complexity of a chaotic waveform. One is the correlation dimension that increases with the complexity of the chaotic state. The numerical methods for calculating the Lyapunov exponents in the time domain and the correlation dimension of the chaotic attractor in the phase space are discussed in Section 9.3.

Although the complexity of a chaotic waveform is important, the ability to stably synchronize two nonlinear dynamical systems serving as transmitter and receiver, respectively, is a key issue for synchronized chaotic communications. Theoretically, perfect synchronization requires a perfect match in the parameters of the transmitter and the receiver being synchronized. Although allowing for perfect synchronization, perfect parameter matching does not guarantee the stability of synchronization against noise or any other form of perturbation. The robustness of chaos synchronization can be examined by finding the transverse Lyapunov exponents of the synchronized chaotic trace. Perfect parameter matching is generally not possible for real systems. Therefore, the concept of transverse Lyapunov exponents for perfect synchronization has to be modified for real systems that have parameter mismatch. These concepts and the numerical methods developed for quantifying the robustness and quality of synchronization are discussed in Section 9.4.

All of the numerical methods discussed in this chapter focus on nonlinear systems that are described by differential equations though some of them can be generalized to systems described by mapping equations, such as the tent map or the logistic map systems. Optically injected semiconductor lasers are used as examples to demonstrate the numerical methods addressed in this chapter. The dynamics and synchronization of such lasers are thoroughly discussed in Chapter 10. The examples in this chapter demonstrate the application of the numerical methods to these lasers.

## 9.2 Numerical Simulation of Stochastic Differential Equations

It is necessary to consider noise in the simulation of a realistic system because noise always exists in any physical system. For a nonlinear dynamical system, such as a semiconductor laser, noise is not simply a linear addition to the dynamics but is an integral part of the dynamics. The expression of noise is subject to the nonlinearity in the system, but noise also affects the dynamics of the system on the other hand. For a communication system, noise is a key factor that determines the performance of the system. Specially, because the communication systems discussed here are nonlinear systems, the effect of noise on the system performance is also nonlinear. The method of dealing with channel noise in traditional communication systems cannot be used in chaotic communications.

The difference between the simulation of a regular differential equation and that of a stochastic differential equation is that noise is always random and nondeterministic. When solving a stochastic differential equation, the actual value of noise at any moment is not known. The effect of noise can only be evaluated through an ensemble average. Therefore, the rule of the Riemann–Stieltjes integral that treats the integrand as a deterministic function of time does not apply in the integration of a stochastic differential equation that contains one or more noise terms. For this reason, the numerical method for solving stochastic nonlinear differential equations has to be treated with extra care. Instead of the Riemann–Stieltjes integral, a stochastic integral is considered in the numerical analysis.

In general, there are two different methods to calculate a stochastic integral, namely, the Ito integral and the Stratonovich integral. The Ito integral assumes that the correlation time between random processes is zero; it is designed for calculating a stochastic integral with white noise. The Stratonovich integral assumes that a correlation exists between random processes at different moments; it is designed for color noise. The difference between the Ito integral and the Stratonovich integral can be very significant [1]. Which integral has to be chosen depends on the correlation characteristic of the noise under consideration. Detailed discussions regarding these integrals are presented in this section.

Semiconductor laser systems are used as examples in this chapter to demonstrate the numerical concepts. Because the semiconductor lasers functioning as the chaotic oscillators have spontaneous emission as the noise source, all of the equations that describe the nonlinear dynamics, the chaos synchronization, and the chaotic communication are stochastic nonlinear differential equations. In general, the noise sources of semiconductor lasers include the optical noise from spontaneous emission and the carrier noise. The optical noise is white Gaussian noise, and the carrier noise is color noise. The carrier noise is ignored in the numerical analysis of a single-mode laser because this narrowband color noise is contributed mainly by the partition noise

of the side modes [2,3]. Therefore, when single-mode semiconductor lasers are considered, only optical noise from spontaneous emission with a white Gaussian nature is included. The discussions in the following are thus limited to white Gaussian noise sources.

### 9.2.1 Langevin Equation

The rate equations of a system with white noise sources can be generalized in the following form of stochastic differential equations, known as the vector Langevin equation [4–10],

$$\frac{dx_i}{dt} = f_i(\mathbf{x}, t) + \sum_{j=1}^k g_{ij}(\mathbf{x}, t)n_j(t), \quad (9.1)$$

where  $i = 1, \dots, m$  is the dimension index of the differential equation, and  $j = 1, \dots, k$  is the index of the stochastic sources. In this equation, both  $f_i(\mathbf{x}, t)$  and  $g_{ij}(\mathbf{x}, t)$  are deterministic functions but  $n_j(t)$  represents a stochastic process. This equation was provided by Langevin to explain the Brownian motion besides Einstein's explanation, which is a special case of the Fokker–Planck equation. The stochastic term  $n_j(t)$  is independent white Gaussian noise that has the following properties,

$$\langle n_j(t) \rangle = 0, \quad (9.2)$$

$$\langle n_i(t)n_j(t - \tau) \rangle = \delta_{ij}\delta(\tau), \quad (9.3)$$

where  $\langle \cdot \rangle$  means ensemble average. Because of  $\delta_{ij}$  on the right-hand side of (9.3),  $\langle n_i(t)n_j(t - \tau) \rangle$  is an autocorrelation function. For demonstration purposes, the discussions are focused on a one-dimensional Langevin equation with a single white Gaussian noise term, that is, a scalar Langevin equation, as follows,

$$\frac{dx}{dt} = f(x, t) + g(x, t)n(t). \quad (9.4)$$

The discussions on the scalar Langevin equation can be generally applied to the vector Langevin equation.

For the differential equation written in the form of (9.4) above, we would suppose that  $n(t)$  is integratable and thus the integral

$$W(t) = \int_0^t n(s)ds \quad (9.5)$$

exists. This integral is actually a Wiener process, denoted by  $W(t)$ , which belongs to a larger subclass of the stochastic process known as the Markov process, or simply Markovian. This means that a Wiener process is memoryless. The Wiener process has the following properties,

$$W(0) = 0, \quad (9.6)$$

$$\langle W(t) \rangle = 0, \quad (9.7)$$

$$\text{Var}[W(t) - W(s)] = t - s, \quad \text{for all } 0 \leq s \leq t, \quad (9.8)$$

where  $\text{Var}[\cdot]$  stands for variance. From this standard definition of the Wiener process, we obtain the relationship that  $\text{Var}[W(t) - W(s)] = E\{[W(t) - W(s)]^2\} = t - s$  because  $\langle W(t) \rangle = 0$ , where  $E\{\cdot\}$  stands for expectation value. Although random variables are not differentiable in the sense of ordinary calculus, one of the important characteristics of the Wiener process is that it is not differentiable even in the sense of the mean-square limit [8, 9]. This property can be seen by examining the convergence of its derivative in the mean-square limit [9]:

$$\left\langle \left[ \frac{W(t+h) - W(t)}{h} \right]^2 \right\rangle = \frac{\langle [W(t+h) - W(t)]^2 \rangle}{h^2} = \frac{1}{h}, \quad (9.9)$$

and, therefore,

$$\lim_{h \rightarrow 0} \left\langle \left[ \frac{W(t+h) - W(t)}{h} \right]^2 \right\rangle = \infty. \quad (9.10)$$

As we can see here, the derivative of  $W(t)$  diverges. The paradox here is that  $W(t)$  is the integral of  $n(t)$ , but itself is not differentiable even in the sense of the mean-square limit.

Because  $x(t)$  is a real physical observable but the time derivative of  $x(t)$  is not, the fact that  $W(t)$  is not differentiable means that, mathematically speaking, a Langevin equation does not exist. Its use is only in the sense of physical intuition. The question here is the following: If a Langevin equation does not exist in the mathematical sense, can it be modified to be self-consistent? By examining some properties of the Wiener process  $W(t)$ , it is important to understand that the Wiener process is not a stationary process in both the strict and the wide senses: As we know, the conditional probability of the Wiener process is [10]

$$p(W_i, t_i | W_{i-1}, t_{i-1}) = \frac{1}{\sqrt{4\pi D(t_i - t_{i-1})}} \exp\left[-\frac{(W_i - W_{i-1})^2}{4D(t_i - t_{i-1})}\right], \quad (9.11)$$

where  $D$  specifies the increasing rate of its variance [10], which is  $2Dt_i$ . For the Wiener process discussed here, we have  $D = 1$ . By choosing the initial condition  $p(W_0, t_0 = 0) = \delta(W_0)$ , the probability density for  $t \geq 0$  is

$$p_1(W, t) = \int p(W, t | W_0, t_0 = 0) \delta(W_0) dW_0 = \frac{1}{4\pi Dt} \exp\left(-\frac{W^2}{4Dt}\right), \quad (9.12)$$

which is dependent on time. Therefore, it is not a stationary process in the strict sense. From the probability density  $p_1(W, t)$ , we can also prove that the first moment vanishes,  $\langle W(t) \rangle = 0$ , and that  $\langle W(t_1)W(t_2) \rangle = 2D \min(t_1, t_2)$ .

From here, it can also be concluded that it is not a stationary process in the wide sense, either.

However, the increments,  $\Delta W_{t_1, t_2} \equiv W_{t_2} - W_{t_1}$ , of the Wiener process are stationary. The Wiener process can be represented as a continuous sum over subsequent independent increments:

$$W(t) = \sum_{i=1}^n (\Delta W_{t_{k+1}-t_k}). \quad (9.13)$$

The integral  $W(t) = \int^t dW(s)$  as defined by the sum of the increments of the Wiener process is then well-defined. Then, the integral of (9.4) in the form of

$$x(t) - x(t_0) = \int_{t_0}^t f(x, s)ds + \int_{t_0}^t g(x, s)n(s)ds \quad (9.14)$$

can be interpreted consistently by a replacement of  $n(t)dt$ , which is made by directly following the interpretation of the integral of  $n(t)$ , as the Wiener process  $W(t)$ :

$$dW(t) \equiv W(t + dt) - W(t) = n(t)dt. \quad (9.15)$$

The integral equation in (9.14) can then be rewritten as

$$x(t) - x(t_0) = \int_{t_0}^t f(x, s)ds + \int_{t_0}^t g(x, s)dW(s), \quad (9.16)$$

where  $f(x, t)$  is called the *drift* term of the stochastic integral equation, and  $g(x, t)$  is called the *diffusion* term. Under this replacement, the integral for  $n(t)$  can be defined through the integration of  $dW(t)$ . Equation (9.16) is named as a stochastic integral equation.

The stochastic integral expressed in (9.16) is very different from a deterministic Riemann–Stieltjes integral. To simplify the discussion, let us consider the integral in the form of

$$x(t_0 + h) - x(t_0) = \int_{t_0}^{t_0+h} u(s)ds, \quad (9.17)$$

where  $h$  is a very small time interval and the integrand  $u(t)$  can be either a deterministic function or a stochastic process. When it is a deterministic function,  $u(t) = f(t)$ , then

$$x(t_0 + h) - x(t_0) \simeq f(t_0)h. \quad (9.18)$$

That is to say that  $\Delta x \propto h$ . However, when  $u(t)$  is a stochastic process, the result is very different. For example, let us assume that  $u(t)$  is a white Gaussian process with a unity standard deviation that  $u(t) = n(t)$ . The displacement  $x(t_0 + h) - x(t_0)$  is then obtained as the following,

$$\begin{aligned}
x(t_0 + h) - x(t_0) &= \int_{t_0}^{t_0+h} n(s)ds = \int_{t_0}^{t_0+h} dW(s) \\
&\simeq \Delta W_{t_0+h,t_0} \\
&\simeq \sqrt{h} Y,
\end{aligned} \tag{9.19}$$

where  $Y$  is a Gaussian variable with a zero mean and a unity standard deviation. This result can be realized by the fact that the average of  $\Delta W_{t_0+h,t_0}$  is zero, and

$$\text{Var}(\Delta W_{t_0+h,t_0}) = \langle (\Delta W_{t_0+h,t_0})^2 \rangle = h. \tag{9.20}$$

As is obtained in (9.19), the displacement,  $\Delta x = x(t_0 + h) - x(t_0)$ , is proportional to  $\sqrt{h}$  in the case of a stochastic process. The integral proportional to  $\sqrt{h}$  is the result of the integral in the sense of the expectation value. An example that demonstrates the difference between using  $\sqrt{h}$  and  $h$  to solve a stochastic integral equation can be found in [1]. In contrast, the Riemann–Stieltjes integral yields the same result proportional to  $h$  in both the regular convergence limit and the mean-square convergence limit.

In this subsection, we clarify the critical difference between a deterministic integral and a stochastic integral. Based on the different definitions to calculate the stochastic integral, however, we have a stochastic integral in the Ito sense and that in the Stratonovich sense. Which one has to be used depends on the characteristics of the noise source, which in turn depends on the problem being considered.

### 9.2.2 Stochastic Integral

The first integral on the right-hand side of (9.16) is a deterministic integral, which is a Riemann–Stieltjes integral, and it is not of concern here. Thus, we only focus on the second integral in (9.16) at this moment, which is stochastic. A discussion to cover the entire evaluation of the integral equation is addressed in the next subsection when the concept of the stochastic integral is implemented in numerical analysis.

Now suppose that the function  $u(t)$  is an arbitrary function, and  $W(t)$  is the Wiener process. The stochastic integral can be defined in a manner similar to the Riemann–Stieltjes integral, but not the same in the sense of convergence criteria. We divide the interval  $[t_0, t]$  into  $n$  subdivisions with the order  $t_0 \leq t_1 \leq t_2 \leq \dots \leq t_{n-1} \leq t_n = t$  and define intermediate points  $\tau_i$ , where the function  $u(t)$  is evaluated, such that

$$t_{i-1} \leq \tau_i \leq t_i. \tag{9.21}$$

The stochastic integral can be defined as the limit of the partial sums:

$$S_n = \sum_{i=1}^n u(\tau_i)[W(t_i) - W(t_{i-1})]. \tag{9.22}$$

The limit applied here is in the sense of mean-square limit, which is defined as [9]

$$\lim_{n \rightarrow \infty} \left\langle \left[ S_n - \int_{t_0}^t u(s) dW(s) \right]^2 \right\rangle = 0. \quad (9.23)$$

This definition of the stochastic integral is more general than the second integral term in (9.16). It allows  $u(t)$  to be a stochastic process.

The value of the stochastic integral depends on the choice of the intermediate points  $\tau_i$ . As a common example, let the function  $u(t)$  be replaced by the Wiener process  $W(t)$  [1, 8, 9]. When  $\tau_i = t_{i-1}$ ,

$$\int_{t_0}^t W(s) dW(s) = \frac{1}{2}[W^2(t) - W^2(t_0) - (t - t_0)]. \quad (9.24)$$

However, when  $\tau_i = \frac{1}{2}(t_{i-1} + t_i)$ ,

$$\int_{t_0}^t W(s) dW(s) = \frac{1}{2}[W^2(t) - W^2(t_0)]. \quad (9.25)$$

The stochastic integral (9.24) that is evaluated at  $\tau_i = t_{i-1}$  is an Ito integral, whereas the stochastic integral (9.25) that is evaluated at  $\tau_i = (t_{i-1} + t_i)/2$  is a Stratonovich integral. These two integrals clearly have different results.

The Ito integral, denoted by (I) in front of the integral, is defined as

$$(I) \int_{t_0}^t u(s) dW(s) \equiv \lim_{n \rightarrow \infty} \sum_{i=1}^n u(t_{i-1})(W(t_i) - W(t_{i-1})). \quad (9.26)$$

The Stratonovich integral, denoted by (S) in front of the integral, is defined as

$$(S) \int_{t_0}^t u(s) dW(s) \equiv \lim_{n \rightarrow \infty} \sum_{i=1}^n u\left(\frac{t_{i-1} + t_i}{2}\right)(W(t_i) - W(t_{i-1})). \quad (9.27)$$

The major differences between the Ito integral and the Stratonovich integral are summarized in Table 9.1.

**Table 9.1. Characteristics of Ito and Stratonovich Integrals**

Characteristics	Ito	Stratonovich
Relationship between $u(t_{i-1})$ and $\Delta W_{i,i-1}$	Independent	Dependent
Noise characteristics	True white noise	Color noise
Operation method	Ito calculus	Ordinary calculus

It is important to know that the Ito integral is mathematically more satisfactory, but it is not always the physically natural choice. When the noise  $n(t)$

is realistic noise with a finite correlation time, not a white noise, it is more natural to choose the Stratonovich integral. Furthermore, the Stratonovich integral enables us to use ordinary calculus, which is not possible for the integral in the Ito sense. However, there is the following simple relationship between the integral equation solved in the Ito sense and that solved in the Stratonovich sense [8, 9], in which  $u(t) = g(x, t)$  is a deterministic function,

$$x(t) = x(t_0) + \int_{t_0}^t f(x, s)ds + (\text{I}) \int_{t_0}^t g(x, s)dW(s), \quad (9.28)$$

$$x(t) = x(t_0) + \int_{t_0}^t \bar{f}(x, s)ds + (\text{S}) \int_{t_0}^t g(x, s)dW(s), \quad (9.29)$$

with the modified drift term  $\bar{f}(x, s)$  defined as follows

$$\bar{f}(x, s) = f(x, s) - \frac{1}{2}g(x, s)\frac{\partial g(x, s)}{\partial x}. \quad (9.30)$$

This relationship is only valid in the integral equation, but not in the stochastic integral itself. When the diffusion term,  $g(x, t)$ , is a constant, the Ito integral and the Stratonovich integral are the same. This conclusion can be observed in (9.30) or, alternatively, from a logical intuition that a constant  $g(x, t)$  is always independent of  $\Delta W(t)$ . This is a very important characteristic that serves as an important guideline for programming the simulation of the differential equations of a noisy system.

### 9.2.3 Numerical Algorithm

It is usually easier to start the computer algorithm for the stochastic integral in the Stratonovich sense than in the Ito sense because the integral in the Stratonovich sense follows the ordinary calculus. However, it is still usually complicated even in the Stratonovich sense. In order to apply the theory of the stochastic integral to the differential equations of a noisy nonlinear system, it is more practical to go back to the vector Langevin equation in the integral form, which can be obtained by integrating (9.1), with an additional assumption that  $g_{ij} = \delta_{ij}g_j$ . This assumes that each dynamical variable,  $x_i(t)$ , is contaminated only by a single noise source.

To construct the algorithm, it is necessary to use a small time interval  $\Delta t = h$  in the integral:

$$x_i(h) = x_i(0) + \int_0^h f_i(\mathbf{x}(t))dt + \int_0^h g_i(\mathbf{x}(t))dW_i(t). \quad (9.31)$$

Note that it is necessary to carry out the expansion in terms of the powers of  $h^{1/2}$  rather than in those of  $h$  because  $\Delta W_{t+h,h} \propto h^{1/2}$ . The expansion of  $x_i(h)$  can be obtained by the iteration method [4] as

$$x_i(h) = x_i(0) + \delta x_i^{1/2} + \delta x_i^1 + \delta x_i^{3/2} + \delta x_i^2 + \dots, \quad (9.32)$$

where

$$\delta x_i^{1/2} = g_i Z_{1,i}, \quad (9.33)$$

$$\delta x_i^1 = f_i h + \frac{1}{2} \sum_j g_{i,j} g_j Z_{1,i} Z_{1,j}, \quad (9.34)$$

$$\begin{aligned} \delta x_i^{3/2} &= \sum_j (f_{i,j} g_j Z_{2,j} - g_{i,j} f_j Z_{2,i}) + \frac{1}{3!} \sum_{j,k} g_{i,j} g_{j,k} g_k Z_{1,i} Z_{1,j} Z_{1,k} \\ &\quad + \sum_j g_{i,j} f_j h Z_{1,i} + \frac{1}{6} \sum_{j,k} g_{i,j,k} g_j g_k Z_{1,i} Z_{1,j} Z_{1,k}, \end{aligned} \quad (9.35)$$

$$\begin{aligned} \delta x_i^2 &= \frac{1}{2} \sum_j f_{i,j} f_j h^2 + \frac{1}{2} \sum_{j,k} f_{i,j} g_{j,k} g_k Z_{3,jk} + \frac{1}{2} \sum_{j,k} f_{i,j,k} g_j g_k Z_{3,jk} \\ &\quad + \sum_{j,k} g_{i,j} \{ [f_{j,k} g_k (Z_{1,i} Z_{2,k} - Z_{3,ik}) - g_{j,k} f_k (Z_{1,i} Z_{2,j} - Z_{3,ij})] \\ &\quad + \frac{1}{2} g_{j,k} f_k (h Z_{1,i} Z_{1,j} - Z_{3,ij}) \} \\ &\quad + \frac{1}{24} \sum_{j,k,l} g_{i,j} g_{j,k} g_{k,l} g_l Z_{1,i} Z_{1,j} Z_{1,k} Z_{1,l} \\ &\quad + \frac{1}{2} \sum_{j,k} g_{i,j,k} g_k [\frac{1}{2} f_j (h Z_{1,i} Z_{1,k} - Z_{3,ik}) + \frac{1}{8} Z_{1,i} Z_{1,j} Z_{1,k} \sum_l g_{j,l} g_l Z_{1,l}] \\ &\quad + \frac{1}{24} \sum_{j,k,l} g_{i,j,k,l} g_j g_k g_l Z_{1,i} Z_{1,j} Z_{1,k} Z_{1,l} \\ &\quad + \frac{1}{24} \sum_{l,j,k} g_{i,l} g_{l,j,k} g_j g_k Z_{1,i} Z_{1,j} Z_{1,k} Z_{1,l}, \end{aligned} \quad (9.36)$$

where  $f_i \equiv f_i(\mathbf{x}_0)$ ,  $g_i \equiv g_i(\mathbf{x}_0)$ ,  $g_{i,j} \equiv \frac{\partial}{\partial x_j} g_i(\mathbf{x}_0)$ ,  $g_{i,j,k} \equiv \frac{\partial^2}{\partial x_j \partial x_k} g_i(\mathbf{x}_0)$ ,  $f_{i,j} \equiv \frac{\partial}{\partial x_j} f_i(\mathbf{x}_0)$ , and  $f_{i,j,k} \equiv \frac{\partial^2}{\partial x_j \partial x_k} f_i(\mathbf{x}_0)$ , and  $Z_{1,i}$ ,  $Z_{2,i}$ , and  $Z_{3,ij}$  are defined as follows,

$$Z_{1,i} \equiv \int_0^h dW_i(t), \quad (9.37)$$

$$Z_{2,i} \equiv \int_0^h \left[ \int_0^t dW_i(s) \right] dt, \quad (9.38)$$

$$Z_{3,ij} \equiv \int_0^h \left[ \int_0^t dW_i(s) \int_0^t dW_j(s) \right] dt. \quad (9.39)$$

As we can see above, the expansion is complicated. And it is still the integral in the Stratonovich sense rather than that in the Ito sense. However, when

$g_i(\mathbf{x}, t)$  is a constant, the terms in the expansion are reduced to the following simple expressions,

$$\delta x_i^{1/2} = g_i Z_{1,i}, \quad (9.40)$$

$$\delta x_i^1 = f_i h, \quad (9.41)$$

$$\delta x_i^{3/2} = \sum_j f_{i,j} g_j Z_{2,j}, \quad (9.42)$$

$$\delta x_i^2 = \frac{1}{2} \sum_j f_{i,j} f_j h^2 + \frac{1}{2} \sum_{j,k} f_{i,jk} g_j g_k Z_{3,jk}. \quad (9.43)$$

We thus have

$$x_i(h) = x_i(0) + h f_i + \frac{1}{2} h^2 \sum_j f_{i,j} f_j + \dots + S_i, \quad (9.44)$$

$$S_i = g_i Z_{1,i} + \sum_j f_{i,j} g_j Z_{2,j} + \frac{1}{2} \sum_{j,k} f_{i,jk} g_j g_k Z_{3,jk} + \dots \quad (9.45)$$

Meanwhile, the stochastic integral in the Ito sense is the same as that in the Stratonovich sense when  $g_i$  is a constant. Therefore, it is most desirable that the differential equations modeling a system contain only constant diffusion terms with  $g_i$  being independent of both  $\mathbf{x}$  and  $t$ . In order to carry out the algorithm numerically, a further step has to be established to avoid precalculation on the partial derivative of  $f_i$  in (9.41), (9.42), and (9.43). In general, Runge–Kutta method is used for this purpose. The detailed discussion can be found in [6].

#### 9.2.4 Example: Dynamics of an Optically Injected Semiconductor Laser

We now use a single-mode semiconductor laser subject to optical injection as an example to demonstrate the simulation of the stochastic differential equations. Detailed discussions of the dynamics of this system can be found in Subsection 7.4.1 of Chapter 7. Here we concentrate on the mathematical aspects of formulating the differential equations for numerical simulation and the effect of noise on the dynamical characteristics of the system seen from the numerical results.

The dynamics of a semiconductor laser subject to the injection of an optical field is mathematically modeled by the following coupled equations [11],

$$\frac{dA}{dt} = -\frac{\gamma_c}{2} A + i(\omega_0 - \omega_c) A + \frac{\Gamma}{2}(1 - ib) g A + \eta A_i \exp(-i\Omega t) + F_{sp}, \quad (9.46)$$

$$\frac{dN}{dt} = \frac{J}{ed} - \gamma_s N - \frac{2\epsilon_0 n^2}{\hbar\omega_0} g |A|^2, \quad (9.47)$$

where  $A$  is the total complex intracavity field amplitude of the laser at its free-oscillating frequency  $\omega_0$  and  $N$  is the carrier density. The injection field has a complex amplitude of  $A_i$  at an optical frequency of  $\omega_i$ , which is detuned from the free-running frequency  $\omega_0$  of the injected laser by a detuning frequency of  $\Omega = \omega_i - \omega_0 = 2\pi f$ . Other variables in these coupled equations are defined in Chapter 10. The noise term,  $F_{sp}(t)$ , which originates from the spontaneous emission of the semiconductor laser, is described by a complex Langevin source term,  $F_{sp}(t) = F_r(t) + iF_i(t)$ . It is white Gaussian noise that is characterized by the following correlation relations [2,3],

$$\langle F_r(t)F_r(t') \rangle = \langle F_i(t)F_i(t') \rangle = \frac{R_{sp}}{2} \delta(t - t') , \quad (9.48)$$

$$\langle F_r(t)F_i(t') \rangle = 0 , \quad (9.49)$$

where  $R_{sp}$  is the spontaneous emission rate. The focus of the discussions in the following is placed on the stochastic term of the spontaneous emission noise  $F_{sp}(t)$ . Other terms are all deterministic.

By writing  $A$  in terms of its magnitude and phase as  $A = |A_0|(1+a)e^{i\varphi}$ , and  $N$  as  $N = N_0(1+\tilde{n})$ , these two coupled rate equations can be transformed into the following three coupled equations [12],

$$\begin{aligned} \frac{da}{dt} &= \frac{1}{2} \left[ \frac{\gamma_c \gamma_n}{\gamma_s \tilde{J}} \tilde{n} - \gamma_p (2a + a^2) \right] (1+a) + \xi \gamma_c \cos(2\pi ft + \varphi) \\ &\quad + \frac{F_r \cos \varphi + F_i \sin \varphi}{|A_0|} , \end{aligned} \quad (9.50)$$

$$\begin{aligned} \frac{d\varphi}{dt} &= -\frac{b}{2} \left[ \frac{\gamma_c \gamma_n}{\gamma_s \tilde{J}} \tilde{n} - \gamma_p (2a + a^2) \right] - \frac{\xi \gamma_c}{1+a} \sin(2\pi ft + \varphi) \\ &\quad - \frac{1}{1+a} \frac{F_r \sin \varphi - F_i \cos \varphi}{|A_0|} , \end{aligned} \quad (9.51)$$

$$\begin{aligned} \frac{d\tilde{n}}{dt} &= -\gamma_s \tilde{n} - \gamma_n \tilde{n} (1+a)^2 - \gamma_s \tilde{J} (2a + a^2) \\ &\quad + \frac{\gamma_s \gamma_p}{\gamma_c} \tilde{J} (2a + a^2) (1+a)^2 . \end{aligned} \quad (9.52)$$

We can use an orthogonal transformation to further simplify the noise terms in (9.50) and (9.51) into  $F_a = (F_r \cos \varphi + F_i \sin \varphi)/|A_0|$  and  $F_\varphi = -(F_r \sin \varphi - F_i \cos \varphi)/|A_0|$ , respectively, in which  $F_a$  and  $F_\varphi$  are still white Gaussian. However, the noise term in the phase equation (9.51) still contains a nonconstant factor of the form

$$\frac{1}{1+a(t)} \quad (9.53)$$

that depends on the variable  $a(t)$ . Thus, recasting the coupled equations into the three equations given in (9.50)–(9.52) does not result in the most convenient form for numerical analysis when the laser noise is considered.

Instead of the amplitude  $a$  and the phase  $\varphi$ , the real and imaginary parts of  $A/|A_0|$  defined by  $A = |A_0|(a' + ia'')$  can be used together with  $\tilde{n}$  defined by  $N = N_0(1 + \tilde{n})$  to recast the coupled equations into the following form,

$$\begin{aligned} \frac{da'}{dt} &= \frac{1}{2} \left[ \frac{\gamma_c \gamma_n}{\gamma_s \tilde{J}} \tilde{n} - \gamma_p (a'^2 + a''^2 - 1) \right] (a' + ba'') + \xi \gamma_c \cos(2\pi ft) \\ &\quad + \frac{F_r}{|A_0|}, \end{aligned} \quad (9.54)$$

$$\begin{aligned} \frac{da''}{dt} &= \frac{1}{2} \left[ \frac{\gamma_c \gamma_n}{\gamma_s \tilde{J}} \tilde{n} - \gamma_p (a'^2 + a''^2 - 1) \right] (-ba' + a'') - \xi \gamma_c \sin(2\pi ft) \\ &\quad + \frac{F_i}{|A_0|}, \end{aligned} \quad (9.55)$$

$$\begin{aligned} \frac{d\tilde{n}}{dt} &= -\gamma_s \tilde{n} - \gamma_n \tilde{n} (a'^2 + a''^2) - \gamma_s \tilde{J} (a'^2 + a''^2 - 1) \\ &\quad + \frac{\gamma_s \gamma_p}{\gamma_c} \tilde{J} (a'^2 + a''^2 - 1) (a'^2 + a''^2). \end{aligned} \quad (9.56)$$

Note that  $a' = (1 + a) \cos \varphi$  and  $a'' = (1 + a) \sin \varphi$ , thus  $a'^2 + a''^2 = (1 + a)^2$ , when connecting (9.54) and (9.55) to (9.50) and (9.51). As  $F_r$  and  $F_i$  have the white Gaussian characteristics given in (9.48) and (9.49) and  $|A_0|$  is a constant, we find that the noise terms in these equations both have a constant coefficient of  $g_i = \sqrt{R_{sp}/2|A_0|^2}$  for  $i = 1, 2$  because

$$\frac{F_r}{|A_0|} = \sqrt{\frac{R_{sp}}{2|A_0|^2}} n_1(t) = g_1 n_1(t), \quad (9.57)$$

$$\frac{F_i}{|A_0|} = \sqrt{\frac{R_{sp}}{2|A_0|^2}} n_2(t) = g_2 n_2(t), \quad (9.58)$$

where

$$g_1 = g_2 = \sqrt{\frac{R_{sp}}{2|A_0|^2}}, \quad (9.59)$$

$$\langle n_i(s), n_j(t) \rangle = \delta_{ij} \delta(s - t), \quad (9.60)$$

$$\langle n_i(s) \rangle = 0. \quad (9.61)$$

The constant coefficients  $g_1$  and  $g_2$  for the noise terms reduce the complexity of the computer algorithm. Therefore, these coupled equations are preferred for the numerical simulation of a semiconductor laser subject to optical injection when noise is considered.

We use the bifurcation diagrams, shown in Figures 9.1a and b, to give an overview of the nonlinear effect of noise on the different dynamical states of the system. This diagram is obtained by collecting the extrema of  $a(t) = \sqrt{a'(t)^2 + a''(t)^2 - 1}$  for each operating condition. The numerical simulation is

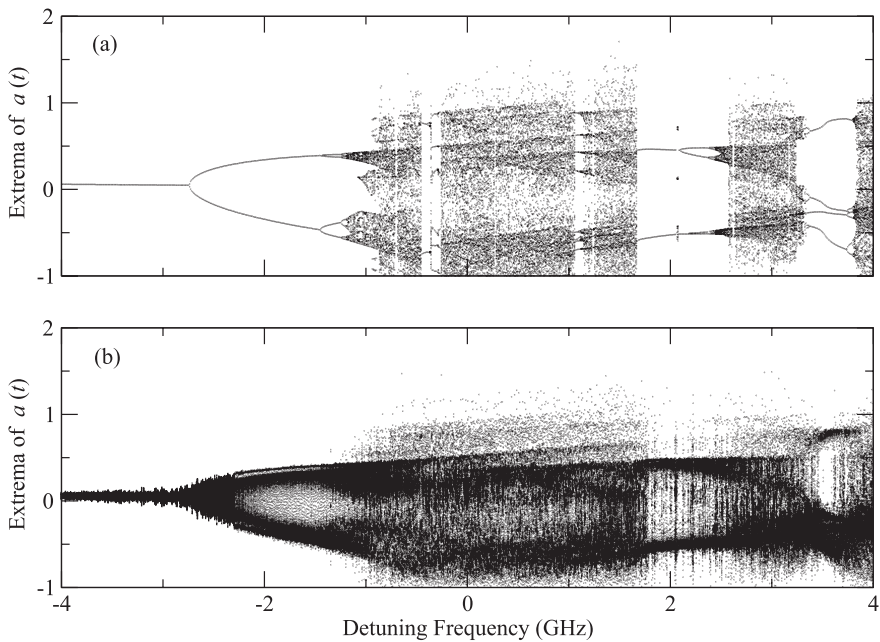


**Fig. 9.1.** Bifurcation diagrams (a) with  $R_{sp} = 0$  and (b) with  $R_{sp} = 4.7 \times 10^{18} \text{ V}^2 \text{m}^{-2} \text{s}^{-1}$  of a semiconductor laser subject to optical injection with an injection parameter of  $\xi = 0.03$  and a detuning frequency varying from  $-4$  GHz to  $4$  GHz.

performed with  $\xi = 0.03$  and  $f$  varying from  $-4$  GHz to  $4$  GHz. The diagram without the consideration of the intrinsic laser noise is shown in Figure 9.1a, and that with the consideration of the noise is shown in Figure 9.1b. The dynamics of this system follows a period-doubling route to chaos [12]. It is seen in Figure 9.1a that the dynamics evolves from a stable locking state at  $f = -4$  GHz through periodic states to chaotic states. When noise is present, it is observed in Figure 9.1b that all the states are blurred by the noise, but some states have dramatic changes in their dynamical characteristics by the noise. For example, the stable locking states and the chaotic states can still be recognized in Figure 9.1b, but some periodic states in windows within the chaos region cannot be easily distinguished from the nearby chaotic states.

Here we use the chaotic state obtained at  $\xi = 0.03$  and  $f = 0$  GHz and the periodic state obtained at  $\xi = 0.03$  and  $f = -0.4$  GHz in one of the windows within the chaos region as examples to demonstrate the nonlinear effect of the noise to different dynamical states. The effect of the noise on the chaotic state at  $\xi = 0.03$  and  $f = 0$  GHz is shown in Figure 9.2. The waveform, attractor,

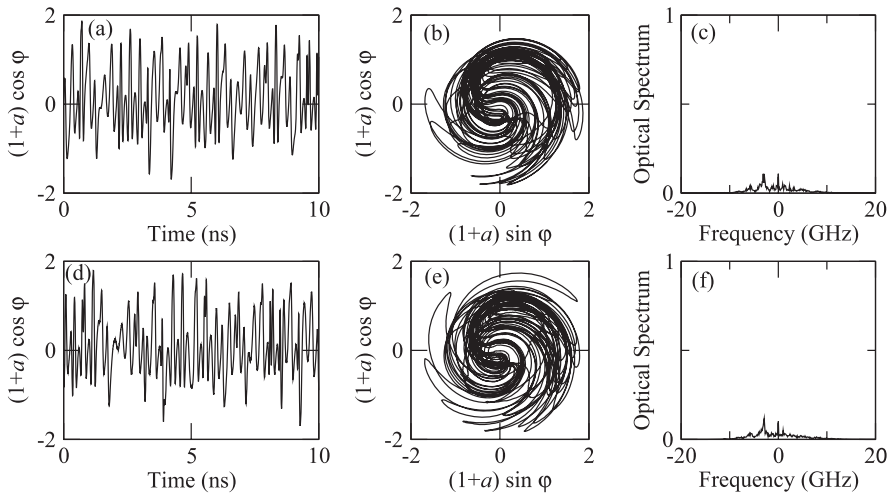


**Fig. 9.2.** Nonlinear effect of intrinsic laser noise on the chaotic state at  $\xi = 0.03$  and  $f = 0$  GHz: (a) Waveform, (b) attractor, and (c) optical spectrum are for  $R_{sp} = 0$ . (d) Waveform, (e) attractor, and (f) optical spectrum are for  $R_{sp} = 4.7 \times 10^{18}$  V<sup>2</sup>m<sup>-2</sup>s<sup>-1</sup>.

and optical spectrum in the absence of noise are shown in Figures 9.2a–c, respectively. The corresponding plots for the system in the same operating condition but in the presence of noise are shown in Figures 9.2d–f. By comparing Figures 9.2a–c with Figures 9.2d–f, the effect of the noise can barely be recognized because the power of the noise is spread in the bandwidth of the chaotic state. In reality, the noise only adds some fluctuations to this chaotic waveform and its attractor. Therefore, it increases the correlation dimension of the chaotic state by contaminating the attractor. This aspect is discussed in Subsection 9.3.4. This characteristic is quite general for the chaotic states in this system.

However, the effect of the noise on some dynamical states can be dramatic if noise-induced order or noise-induced chaos takes place [13]. An example of such effect is demonstrated in Figure 9.3 for  $\xi = 0.03$  and  $f = -0.4$  GHz. Each small plot in Figure 9.3 corresponds to that in Figure 9.2. In the absent of the intrinsic laser noise, the characteristics of this periodic state can be observed from its waveform, attractor, and optical spectrum, shown in Figures 9.3a–c, respectively. However, when noise is present, we find that the system is in a chaotic state with completely different characteristics for its waveform, attractor, and optical spectrum. The examples shown in Figures 9.2 and 9.3 demonstrate that the effect of the noise can be very different for different

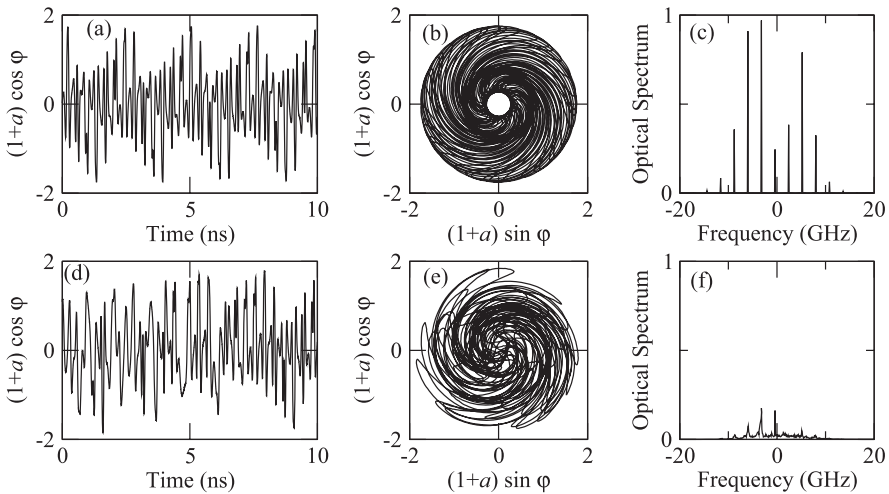


**Fig. 9.3.** Nonlinear effect of intrinsic laser noise on the state, which is periodic in the absence of noise but is chaotic in the presence of noise, at  $\xi = 0.03$  and  $f = -0.4$  GHz: (a) waveform, (b) attractor, and (c) optical spectrum for  $R_{sp} = 0$ ; (d) waveform, (e) attractor, and (f) optical spectrum for  $R_{sp} = 4.7 \times 10^{18} \text{ V}^2 \text{m}^{-2} \text{s}^{-1}$ .

dynamical states. They show that the effect of noise on a nonlinear system is not simply linear and additive but can be highly nonlinear.

### 9.3 Characterization of Chaos

The most fundamental characteristic of chaos is its sensitivity to the initial condition of the dynamical system. When there is a small amount of deviation between two initial conditions, this small deviation will be exponentially enlarged as time evolves. The dynamical system then evolves into different conditions represented by different points in its phase space. This phenomenon is called sensitivity to the initial condition. The corresponding divergence is measured by Lyapunov exponents. The entire trace of the dynamical system forms a chaotic attractor. Chaos occurring in nature is an attractor if the system is dissipative with a confined total energy.

Because of this characteristic, a chaotic attractor in its phase space does not repeat itself. Therefore, the geometric structure is usually fractal though some exception does exist in certain dynamical systems [10]. The divergence also reveals the characteristic of the nonperiodic motion of a chaotic dynamical system. The nonperiodic motion gives a chaotic system a broadband characteristic in the frequency domain. All of these signatures can be used to characterize chaos.

### 9.3.1 Divergence Characterized by Lyapunov Exponents

A dynamical system can be defined by an iterative equation

$$\mathbf{x}(k+1) = \mathbf{F}(\mathbf{x}(k)), \quad (9.62)$$

where  $k = 1, 2, \dots, n$ , or by a differential equation

$$\frac{d\mathbf{x}}{dt} = \mathbf{F}(\mathbf{x}(t)), \quad (9.63)$$

where  $\mathbf{x}(k)$  and  $\mathbf{x}(t)$  are sets of variables describing the system dynamics. Such variables represented by  $\mathbf{x}(k)$  or  $\mathbf{x}(t)$  span the phase space of the corresponding dynamical system.

What we are concerned with here is the rate of divergence between two traces starting from two initial conditions that are close to each other. First, consider a system described by an iterative equation as given in (9.62). By defining the deviation,  $\mathbf{e}$ , of a neighboring trace away from the original trace as  $\mathbf{e}(k) \equiv \mathbf{x}(k) - \mathbf{x}_0(k)$ , where  $\mathbf{x}_0$  indicates the original trace, we have

$$\begin{aligned} \mathbf{x}_0(k+1) + \mathbf{e}(k+1) &= \mathbf{F}(\mathbf{x}_0(k) + \mathbf{e}(k)) \\ &= \mathbf{F}(\mathbf{x}_0(k)) + \mathbf{DF}(\mathbf{x}_0(k)) \cdot \mathbf{e}(k), \end{aligned} \quad (9.64)$$

where the matrix  $\mathbf{DF}$  is defined as

$$\mathbf{DF}(\mathbf{x}_0(k))_{ij} \equiv \frac{\partial F_i(\mathbf{x}_0(k))}{\partial x_j}. \quad (9.65)$$

Therefore, we obtain

$$\mathbf{e}(k+1) = \mathbf{DF}(\mathbf{x}_0(k)) \cdot \mathbf{e}(k) \quad (9.66)$$

for the iterative equation given in (9.62). Equation (9.66) is called the stability equation. It is important to emphasize that, in calculating the Lyapunov exponents for a system described by an iterative equation, this is the equation form that should be used.

For a system described by a differential equation as given in (9.63), we can obtain the following stability equation through a similar procedure,

$$\frac{d\mathbf{e}}{dt} = \mathbf{DF}(\mathbf{x}_0(t)) \cdot \mathbf{e}(t). \quad (9.67)$$

As can be seen here, the stability equation of the differential equation is different from that of the iterative equation. In order to numerically calculate Lyapunov exponents of a differential equation, one has to convert this stability equation into the form of the stability equation of the iterative equation. This can be achieved by sampling the attractor every  $\tau_s$  time interval at  $t = \tau_s, 2\tau_s, \dots, n\tau_s$ . In the following, we define  $\mathbf{e}(k) = \mathbf{e}(t = k\tau_s)$  for convenience.

The stability equation of the differential equation can then be converted by realizing that (9.67) can be expanded as

$$\frac{\mathbf{e}(k+1) - \mathbf{e}(k)}{\tau_s} \simeq \frac{d\mathbf{e}}{dt} = \mathbf{DF}(\mathbf{x}_0(k)) \cdot \mathbf{e}(k). \quad (9.68)$$

Therefore, we can convert this stability equation into the following form,

$$\begin{aligned} \mathbf{e}(k+1) &= \mathbf{DF}(\mathbf{x}_0(k)) \cdot \mathbf{e}(k) \tau_s + \mathbf{e}(k) \\ &= (\mathbf{I} + \mathbf{DF}(\mathbf{x}_0(k)) \tau_s) \cdot \mathbf{e}(k) \\ &= \mathbf{G}(\mathbf{x}_0(k)) \cdot \mathbf{e}(k), \end{aligned} \quad (9.69)$$

where the matrix  $\mathbf{G}(\mathbf{x}_0(k)) \equiv \mathbf{I} + \mathbf{DF}(\mathbf{x}_0(k)) \tau_s$  and  $\mathbf{I}$  is a unity matrix.

Because most of the publications in the literature only discuss the calculation of the Lyapunov exponents from pure numerical data [16, 17], not from a differential equation, a brief discussion on the calculation of the Lyapunov exponents from a differential equation is provided here. In general, the complex eigenvalues of the Jacobian matrix  $\mathbf{DF}(\mathbf{x}_0(k))$  provide the information of the dynamical stability of the system. The real part of each eigenvalue is a Lyapunov exponent that provides the information of divergence or convergence. The imaginary part provides the information of oscillation or cycling. In order to calculate the Lyapunov exponents of a dynamical system described by a differential equation, we do iteration on the matrix  $\mathbf{G}(\mathbf{x}_0(k))$  instead of diagonalizing the Jacobian  $\mathbf{DF}(\mathbf{x}_0(k))$ . The Lyapunov exponents in the average sense, called the global Lyapunov exponents, can be obtained from the following procedure [16, 17],

$$\begin{aligned} \mathbf{e}(k+L) &= \mathbf{G}(\mathbf{x}_0(k+L-1)) \cdot \mathbf{G}(\mathbf{x}_0(k+L-2)) \cdots \mathbf{G}(\mathbf{x}_0(k)) \mathbf{e}(k) \\ &\equiv \mathbf{G}^L(\mathbf{x}_0(k)) \cdot \mathbf{e}(k), \end{aligned} \quad (9.70)$$

where

$$\mathbf{G}^L(\mathbf{x}_0(k)) \equiv \mathbf{G}(\mathbf{x}_0(k+L-1)) \cdot \mathbf{G}(\mathbf{x}_0(k+L-2)) \cdots \mathbf{G}(\mathbf{x}_0(k)). \quad (9.71)$$

To calculate the real part of the complex eigenvalues of the Jacobian matrix, we actually calculate the eigenvalues of the following matrix:

$$|\mathbf{e}(k+L)|^2 = [\mathbf{G}^L(\mathbf{x}_0(k))]^\dagger \mathbf{G}^L(\mathbf{x}_0(k)) |\mathbf{e}(k)|^2, \quad (9.72)$$

where the symbol  $\dagger$  denotes the complex-conjugate transpose matrix. We then assign  $[\mathbf{G}^L(\mathbf{x}_0(k))]^\dagger \mathbf{G}^L(\mathbf{x}_0(k))$  to a sequence of matrices:

$$\begin{aligned} [\mathbf{G}^L(\mathbf{x}_0(k))]^\dagger \mathbf{G}^L(\mathbf{x}_0(k)) &= \mathbf{G}^\dagger(\mathbf{x}_0(k)) \cdot \mathbf{G}^\dagger(\mathbf{x}_0(k+1)) \cdots \\ &\quad \mathbf{G}^\dagger(\mathbf{x}_0(k+L-1)) \cdot \mathbf{G}(\mathbf{x}_0(k+L-1)) \cdots \\ &\quad \mathbf{G}(\mathbf{x}_0(k+1)) \cdot \mathbf{G}(\mathbf{x}_0(k)) \end{aligned} \quad (9.73)$$

$$\begin{aligned} &= \mathbf{A}(2L) \cdot \mathbf{A}(2L-1) \cdot \mathbf{A}(2L-2) \cdots \\ &\quad \mathbf{A}(3) \cdot \mathbf{A}(2) \cdot \mathbf{A}(1), \end{aligned} \quad (9.74)$$

where

$$\mathbf{G}^\dagger(\mathbf{x}_0(k)) \equiv \mathbf{A}(2L), \quad (9.75)$$

$$\mathbf{G}^\dagger(\mathbf{x}_0(k+1)) \equiv \mathbf{A}(2L-1), \quad (9.76)$$

$$\mathbf{G}^\dagger(\mathbf{x}_0(k+2)) \equiv \mathbf{A}(2L-2), \quad (9.77)$$

...

$$\mathbf{G}(\mathbf{x}_0(k+2)) \equiv \mathbf{A}(3), \quad (9.78)$$

$$\mathbf{G}(\mathbf{x}_0(k+1)) \equiv \mathbf{A}(2), \quad (9.79)$$

$$\mathbf{G}(\mathbf{x}_0(k)) \equiv \mathbf{A}(1). \quad (9.80)$$

In general, the multiplication of these matrices is ill-conditioned. Therefore, the following QR decomposition has to be used,

$$\mathbf{A}(j)\mathbf{Q}(j-1) = \mathbf{Q}(j)\mathbf{R}(j), \quad (9.81)$$

where  $\mathbf{Q}(0) = \mathbf{I}$ , an identity matrix. Following the tedious procedure of QR decomposition, we eventually obtain

$$\mathbf{A}(2L) \cdot \mathbf{A}(2L-1) \cdots \mathbf{A}(2) \cdot \mathbf{A}(1) = \mathbf{Q}(2L) \cdot \mathbf{R}(2L) \cdot \mathbf{R}(2L-1) \cdots \mathbf{R}(1). \quad (9.82)$$

Assume that

$$\begin{aligned} \mathbf{M}_1 &= \mathbf{Q}(2L) \cdot \mathbf{R}(2L) \cdot \mathbf{R}(2L-1) \cdots \mathbf{R}(1) \\ &\equiv \mathbf{Q}_1(2L) \cdot \mathbf{R}_1(2L) \cdot \mathbf{R}_1(2L-1) \cdots \mathbf{R}_1(1), \end{aligned} \quad (9.83)$$

$$\mathbf{M}_2 = \mathbf{Q}_1^\dagger(2L) \cdot \mathbf{M}_1 \cdot \mathbf{Q}_1(2L), \quad (9.84)$$

$$= \mathbf{R}_1(2L) \cdot \mathbf{R}_1(2L-1) \cdots \mathbf{R}_1(1) \cdot \mathbf{Q}_1(2L). \quad (9.85)$$

By assigning  $\mathbf{R}_1(j) \equiv \mathbf{A}_2(j)$  for  $j > 1$  and  $\mathbf{R}_1(1)\mathbf{Q}_1(2L) \equiv \mathbf{A}_2(1)$  and by applying (9.81) and (9.82) in (9.85), we can rewrite  $\mathbf{M}_2$  as

$$\begin{aligned} \mathbf{M}_2 &= \mathbf{A}_2(2L) \cdot \mathbf{A}_2(2L-1) \cdots \mathbf{A}_2(2) \cdot \mathbf{A}_2(1), \\ &= \mathbf{Q}_2(2L) \cdot \mathbf{R}_2(2L) \cdot \mathbf{R}_2(2L-1) \cdots \mathbf{R}_2(1). \end{aligned} \quad (9.86)$$

By repeating this tedious procedure  $K$  times until  $\mathbf{Q}_K(2L)$  approaches an identity matrix with a desired accuracy, we eventually obtain

$$\mathbf{M}_K = \mathbf{Q}_K(2L) \cdot \mathbf{R}_K(2L) \cdot \mathbf{R}_K(2L-1) \cdots \mathbf{R}_K(1). \quad (9.87)$$

Then we have the Lyapunov exponents in average, the global Lyapunov exponents. These global Lyapunov exponents are denoted as  $\bar{\lambda}_i$  and expressed as

$$\bar{\lambda}_i = \frac{1}{2L} \sum_{j=1}^{2L} \ln[(R_K(j))_{ii}], \quad (9.88)$$

where  $(R_K(j))_{ii}$  is the  $i$ th diagonal element of the matrix  $\mathbf{R}_K(j)$ . Because the QR decomposition guarantees the order of  $\bar{\lambda}_1 \geq \bar{\lambda}_2 \geq \cdots \geq \bar{\lambda}_n$ , the largest

global Lyapunov exponent is  $\bar{\lambda}_1$ . This procedure has been programmed to calculate the global Lyapunov exponents of a Lorentz system to check the accuracy. When a positive global Lyapunov exponent exists, the attractor is verified as a chaotic attractor. This procedure is also used to calculate the transverse Lyapunov exponents of synchronized systems, which are discussed in Subsection 9.4.1

When the dimension of the required phase space is too large to be handled by this matrix method in practice, another method can be used to calculate only the largest Lyapunov exponent. It is based on the concept that the largest Lyapunov exponent usually dominates the divergence [13, 18]. Therefore, the magnitude of the deviation  $\mathbf{e}$  can be described as

$$|\mathbf{e}(k + L)| \approx |\mathbf{e}(k)| \exp(\bar{\lambda}_1 L). \quad (9.89)$$

Therefore,  $\bar{\lambda}_1$  can be calculated as

$$\bar{\lambda}_1 \approx \frac{1}{L} \ln \left| \frac{\mathbf{e}(k + L)}{\mathbf{e}(k)} \right|. \quad (9.90)$$

In general,  $\mathbf{e} = \mathbf{x} - \mathbf{x}_0$  in this method is calculated through the reconstruction of  $\mathbf{x}_0$  from the time series of a single dynamical variable of the system. For example, the dynamical variable  $x_i(t)$  as a function of time is chosen to construct the vector  $\mathbf{x}_0$ . This is achieved by assigning  $x_i(t)$  as  $y_1(t)$ ,  $x_i(t + \tau_s)$  as  $y_2(t)$ ,  $x_i(t + 2\tau_s)$  as  $y_3(t)$ , and so forth until the whole set of  $\{y_i(t), i = 1, \dots, d\}$  can represent the dynamics of the attractor. The vectors  $\mathbf{x}_0$  are then constructed as  $\mathbf{x}_0(i) \equiv \mathbf{x}_0(t_i) = \{y_1(t_i), y_2(t_i), \dots, y_{d-1}(t_i), y_d(t_i)\}$ . The phase space expanded by  $\{y_i(t), i = 1, \dots, d\}$  is recognized as the embedding space of the attractor, and  $d$  is the dimension of the embedding space. Whether  $\{y_i(t), i = 1, \dots, d\}$  can represent the entire attractor or not depends on the proper choice of the time lag  $\tau_s$  and the embedding dimension  $d$ . After the attractor is reconstructed in the embedding space, we can choose a point  $\mathbf{x}_0(i)$  as a center, and a set of points  $\mathbf{x}_0(j)$  within a small shell centered at  $\mathbf{x}_0(i)$  as  $\mathbf{x}$ . Thus, the deviation  $\mathbf{e} = \mathbf{x} - \mathbf{x}_0$  can be defined, and the magnitude of  $\mathbf{e}$  is measured as the size of the shell. The set  $\mathbf{x}$  is called the nearest neighboring points. Detailed discussions can be found in [13, 18].

The deviation  $\mathbf{e}(k)$  can also be generated by a perturbation along the transmitter trace in the numerical simulation program. By calculating the average of the convergence or divergence of the perturbation, the largest Lyapunov exponent can be obtained. This method is very similar to the one discussed above for the calculation of the largest Lyapunov exponent. The difference is that this method generates the nearest neighboring points by the perturbation.

### 9.3.2 Geometric Structure Measured by Dimension of Chaotic Attractor

Another method to characterize a chaotic attractor is to characterize its geometric structure measured by dimensions. In general, a chaotic attractor is

also a strange attractor, which means its geometric structure is fractal. There are several methods to characterize the geometric structure of a chaotic attractor. Here we discuss only the correlation dimension, which has been found to be a good characterization of a chaotic dynamical state [19, 20]. This correlation dimension is denoted by  $D_2$ . When  $D_2$  is high, the complexity of the chaotic state is high.

To calculate  $D_2$ , we first define the correlation integral  $C(N, r)$  of a dynamical state as [19]

$$C(N, r) = \frac{1}{N^2} \sum_{i,j=1}^N \theta(r - \|X_i - X_j\|), \quad (9.91)$$

where  $\theta(\cdot)$  is the Heaviside step function,  $X_i$  and  $X_j$  are vectors constructed in an embedding space from the time series of a single or several dynamical variables of the system to represent the attractor,  $N$  is the total number of the vectors, and  $r$  is a prescribed small distance.

The correlation dimension is obtained through the local slope of  $\log C(N, r)$  calculated by

$$\nu(r_i) = \frac{\log C(N, r_{i-1}) - \log C(N, r_{i+1})}{\log r_{i-1} - \log r_{i+1}}. \quad (9.92)$$

The value of  $\nu(r_i)$  at the position where  $\nu(r_i)$  shows a plateau provides the value of the correlation dimension  $D_2$ . This method has been proven to be efficient and has been implemented for different dynamical systems [13].

### 9.3.3 Other Signatures

Because most of the data collected for a dynamical system are contaminated by noise in a real world, it is usually difficult to verify from a single signature if the dynamics of a system is chaos or just a diffusion process. Several pieces of evidence have to be collected to make a correct judgment. Besides the Lyapunov exponents and the correlation dimension, a chaotic state can also be verified through the route to chaos. The common routes to chaos are the period-doubling route to chaos, the quasiperiodicity route to chaos, and the intermittency route to chaos. In addition, we can also check the frequency spectrum of a chaotic attractor to obtain another piece of evidence for confirming a chaotic state. Using all these signatures to verify a chaotic state is demonstrated in the following example.

### 9.3.4 Example: Chaos in an Optically Injected Semiconductor Laser

Here we use the chaotic state of the optical injection system operated at  $\xi = 0.03$  and  $f = 0$  GHz to demonstrate the use of the signatures. The route to this chaotic state by varying the detuning frequency is shown in the

bifurcation diagram in Figure 9.1, which is shown in gray in Figure 9.4. This plot shows that the system dynamics evolves from a fixed point at  $f = -4$  GHz through period-one, period-two, and period-four states, as the detuning frequency  $f$  is varied, and finally to the chaotic state at  $f = 0$  GHz.

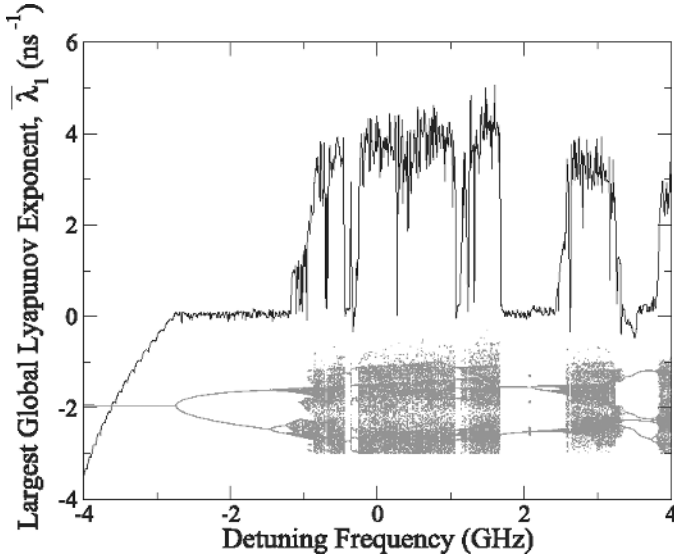


**Fig. 9.4.** Largest global Lyapunov exponent of the dynamical states as a function of detuning frequency ranging from  $f = -4$  GHz to  $f = 4$  GHz with the injection factor being  $\xi = 0.03$ . The gray line is the corresponding bifurcation diagram shown in Figure 9.1a.

Based on the procedure discussed in Subsection 9.3.1, the largest global Lyapunov exponent,  $\bar{\lambda}_1$ , is obtained and shown by the solid line in Figure 9.4. Ideally, fixed points should have global Lyapunov exponents being all negative, periodic states should have  $\bar{\lambda}_1$  being zero, and chaotic states should have at least one positive Lyapunov exponent. However, it is usually very difficult to calculate the Lyapunov exponents into the desired accuracy, say exact  $\bar{\lambda}_1 = 0$  for periodic states. Besides, Lyapunov exponents are not dimensionless, but are inversely proportional to the time scale. The numerical value of a Lyapunov exponent changes with time unit though the characteristic time of the dynamics is usually a good choice. Thus, it is usually not conclusive to announce a state being chaos based solely on the existence of a positive largest Lyapunov exponent, especially when the time scale is around the characteristic time of the dynamics, and the numerical value is closed to zero but is positive. As is shown in Figure 9.4, the fixed points have negative  $\bar{\lambda}_1$  when they are not next to the periodic states. The periodic states judged from the bifurcation diagram have  $\bar{\lambda}_1$  not exact zero but around zero, which

depend on the time unit. This judgment can be further confirmed by the fact that  $\bar{\lambda}_1$  is nearly a constant for all the periodic states based on the bifurcation diagram. Therefore, by combining the bifurcation diagram and the Lyapunov exponents, we can say that the dynamical states with  $\bar{\lambda}_1$  significantly larger than the constant part of the solid curve shown in Figure 9.4 are chaotic, including the state with  $\xi = 0.03$  and  $f = 0$  GHz. The chaotic characteristic of this state can also be further examined by its optical spectrum shown in Figure 9.2c, which shows the broadband characteristic of chaos. This provides an additional piece of evidence to verify this chaotic state.

We can also examine the geometric structure of this chaotic state by calculating its correlation dimension  $D_2$ . As is mentioned in Section 9.3.2, the correlation dimension is determined by the plateau of  $\nu(r_i)$ . The  $\nu(r_i)$  curves marked with different embedding dimensions  $d$  are shown in Figure 9.5a. When  $d$  is smaller than  $D_2$ , the plateau parts of the curves saturate to  $d$ , as is seen in the curves with  $d = 1$  and  $d = 2$  in Figure 9.5a. When  $d$  is larger than  $D_2$ , the plateau parts of the curves approximately stay as a constant and do not increase with  $d$ , as is seen in the curves with  $d \geq 3$  in Figure 9.5a. Therefore, the correlation dimension of the chaotic attractor can be obtained from the common flat part of all the slope curves with  $d \geq 3$  in Figure 9.5a. From Figure 9.5a, the correlation dimension of the dynamical state for  $R_{\text{sp}} = 0$  in the absent of noise is measured to be around  $D_2 \simeq 2.4$ .

The plateau is a very important characteristic for the determination of the correlation dimension from these curves. Because the structure of a chaotic attractor is generally fractal, the structure should remain unchanged when one zooms in or zooms out. This is the reason to have the flat part, where the slope of the correlation integral is independent of the correlation scale. However, when the scale being considered is so small that it reaches the small-scale uniformity limited by the device accuracy, the fractal structure disappears. The local slope of each curve then increases due to the contribution of all the noise, which includes the laser noise and the data truncation noise. On the other ends of all the curves, where the scale being considered is so large that the measured range for calculating the correlation dimension does not only cover the local structure but also covers remote structures, the local slope becomes irregular. It can then either increase or decrease, depending on the specific global property of the attractor. Further increasing the scale will make the chaotic attractor indistinguishable from a single point. At this large scale, we obtain the data showing that the dimension of the chaotic attractor is zero for a single point. All these characteristics can be observed in Figure 9.5a. Therefore, the correlation dimension is obtained only from the flat parts of all curves.

When there is noise in the system, the attractor is contaminated by the noise. The  $\nu(r_i)$  curves contaminated by the laser noise measured by  $R_{\text{sp}} = 4.7 \times 10^{18} \text{ V}^2 \text{m}^{-2} \text{s}^{-1}$  and  $R_{\text{sp}} = 2 \times 4.7 \times 10^{18} \text{ V}^2 \text{m}^{-2} \text{s}^{-1}$  are shown in Figures 9.5b and c, respectively. As is seen, the noise increases the plateau level of each  $\nu(r_i)$  curves with  $d \geq 3$  because the dimension of the noise is infinity.

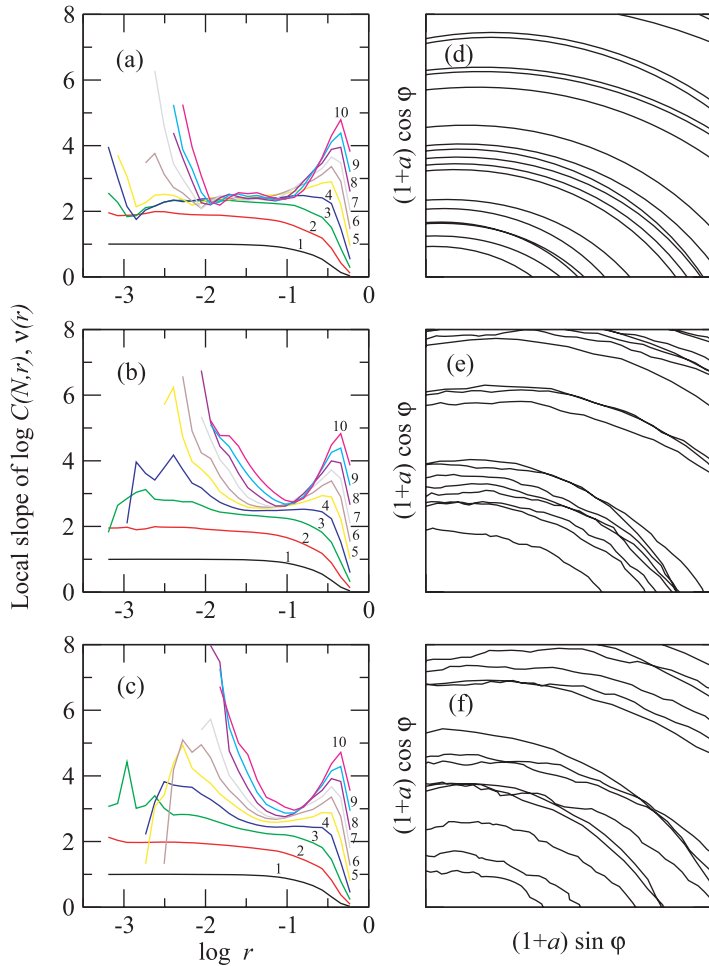


**Fig. 9.5.** Correlation dimension as a function of embedding dimension for the chaotic attractor at  $\xi = 0.03$  and  $f = 0$  GHz with different levels of noise: (a)  $\nu(r_i)$  curves with  $R_{sp} = 0$ ; (b)  $\nu(r_i)$  curves with  $R_{sp} = 4.7 \times 10^{18} \text{ V}^2 \text{m}^{-2} \text{s}^{-1}$ ; (c)  $\nu(r_i)$  curves with  $R_{sp} = 2 \times 4.7 \times 10^{18} \text{ V}^2 \text{m}^{-2} \text{s}^{-1}$ ; (d), (e), and (f) are the portions of the corresponding attractors, respectively. Each  $\nu(r_i)$  curve is marked by the value of its embedding dimension.

Therefore, the common plateau of the  $\nu(r_i)$  curves with  $d \geq 3$  disappears, and it becomes difficult to evaluate  $D_2$ . The local enlargement of the attractors for  $R_{sp} = 4.7 \times 10^{18} \text{ V}^2\text{m}^{-2}\text{s}^{-1}$  and  $R_{sp} = 2 \times 4.7 \times 10^{18} \text{ V}^2\text{m}^{-2}\text{s}^{-1}$  is shown in Figures 9.5e and f, and that of the attractor for  $R_{sp} = 0$  is shown in Figure 9.5d for comparison. The whole attractors with  $R_{sp} = 0$  and  $R_{sp} = 4.7 \times 10^{18} \text{ V}^2\text{m}^{-2}\text{s}^{-1}$  are shown in Figure 9.2b and e, respectively. The effect of the noise with different strength can be observed from the fluctuating traces of the attractor shown in Figures 9.5e and f.

When a dynamical system is contaminated by noise, the verification of its dynamical state becomes more complicated and more difficult. The concept of using several pieces of evidence to verify a chaotic state becomes even more important. The route to chaos provides the unique characteristic of a chaotic system. The bifurcation diagram provides the characteristic of the waveform. The Lyapunov exponents provide the aspect of the sensitivity to the initial condition. The optical spectrum provides the characteristic of the broadband. The correlation dimension  $D_2$  provides the characteristic of the geometric structure. All of these signatures are demonstrated in this example.

## 9.4 Robustness of Chaos Synchronization

The approach to synchronizing chaos considered here is based on the concept described by Kocarev and Parlitz [23]. For two chaotic systems physically connected by a signal  $\mathbf{s}(t)$ , each system can be rewritten mathematically as if the system were driven by a common driving signal  $\mathbf{D}(\mathbf{s}(t))$ , and can be expressed as the following,

$$\frac{d\mathbf{x}}{dt} = \mathbf{F}(\mathbf{x}, \mathbf{D}(\mathbf{s}(t))) , \quad (9.93)$$

$$\frac{d\mathbf{y}}{dt} = \mathbf{G}(\mathbf{y}, \mathbf{D}(\mathbf{s}(t))) , \quad (9.94)$$

where  $\mathbf{D}(\mathbf{s}(t))$  is a function of the signal  $\mathbf{s}(t)$ . With the vector function  $\mathbf{G}$  being equal to the vector function  $\mathbf{F}$ , these two chaotic systems can be synchronized to each other if the difference  $\mathbf{e} = \mathbf{x} - \mathbf{y}$  possesses a fixed point with zero value. This fixed point exists when the average local Lyapunov exponents of the difference  $\mathbf{e}$  are all negative. These average local Lyapunov exponents are also called the average local transverse Lyapunov exponents of the synchronized attractors.

### 9.4.1 Transverse Lyapunov Exponents in the Case of Perfect Parameter Match

Now, we examine the robustness of chaos synchronization by considering the transverse Lyapunov exponents. For illustration purposes, only the additive

driving signal is considered here. In this subsection, only chaos synchronization with perfectly matched parameters is considered, for which  $\mathbf{G} = \mathbf{F}$ . This is an ideal situation that serves the purpose of examining the existence of chaos synchronization.

For synchronization achieved by coupling through an additive driving signal, the general equations (9.93) and (9.94) of the synchronization theory can be rewritten as

$$\frac{d\mathbf{x}}{dt} = \mathbf{F}(\mathbf{x}) + \alpha\mathbf{D}(\mathbf{x}), \quad (9.95)$$

$$\frac{d\mathbf{y}}{dt} = \mathbf{G}(\mathbf{y}) + \alpha\mathbf{D}(\mathbf{x}), \quad (9.96)$$

where  $\alpha\mathbf{D}(\mathbf{x})$  has replaced the driving signal  $\mathbf{s}(t)$  because this special type of driving force is more suitable when the chaos synchronization system is designed for the communication purpose, and the coupling strength  $\alpha$  has been separated from  $\mathbf{s}(t)$ . By defining  $\mathbf{f}(\mathbf{x}) \equiv \mathbf{F}(\mathbf{x}) + \alpha\mathbf{D}(\mathbf{x})$  and  $\mathbf{g}(\mathbf{y}) \equiv \mathbf{G}(\mathbf{y}) + \alpha\mathbf{D}(\mathbf{y})$ , we obtain

$$\frac{d\mathbf{x}}{dt} = \mathbf{F}(\mathbf{x}) + \alpha\mathbf{D}(\mathbf{x}) = \mathbf{f}(\mathbf{x}), \quad (9.97)$$

$$\begin{aligned} \frac{d\mathbf{y}}{dt} &= \mathbf{G}(\mathbf{y}) + \alpha\mathbf{D}(\mathbf{x}) \\ &= \mathbf{G}(\mathbf{y}) + \alpha\mathbf{D}(\mathbf{y}) + \alpha\mathbf{D}(\mathbf{x}) - \alpha\mathbf{D}(\mathbf{y}) \\ &= \mathbf{g}(\mathbf{y}) + \alpha\mathbf{D}(\mathbf{x}) - \alpha\mathbf{D}(\mathbf{y}). \end{aligned} \quad (9.98)$$

When all the parameters are matched,  $\mathbf{G} = \mathbf{F}$  and  $\mathbf{g} = \mathbf{f}$ .

The equations given in (9.97) and (9.98) are the general equations for most of the proposed setups utilizing an additive driving signal to achieve chaos synchronization for the communication purpose. The first equation describes the chaotic dynamics of the transmitter. The second equation describes the synchronization dynamics of the receiver. Now the separation between the traces  $\mathbf{x}(t)$  and  $\mathbf{y}(t)$  is defined as  $\mathbf{e} = \mathbf{y} - \mathbf{x}$ . Then the equation describing the synchronization dynamics can be written as the following,

$$\begin{aligned} \frac{d\mathbf{e}}{dt} &= \mathbf{f}(\mathbf{x} + \mathbf{e}) - \mathbf{f}(\mathbf{x}) - \alpha[\mathbf{D}(\mathbf{x} + \mathbf{e}) - \mathbf{D}(\mathbf{x})] \\ &= \left[ \frac{\partial \mathbf{f}}{\partial \mathbf{x}}(\mathbf{x}) - \alpha \frac{\partial \mathbf{D}}{\partial \mathbf{x}} \right] \cdot \mathbf{e}. \end{aligned} \quad (9.99)$$

By defining  $\mu$  as the eigenvalues of the Jacobian  $\left[ \frac{\partial \mathbf{f}}{\partial \mathbf{x}}(\mathbf{x}) - \alpha \frac{\partial \mathbf{D}}{\partial \mathbf{x}} \right]$ , we obtain the transverse Lyapunov exponents, denoted as  $\lambda_T$ , as the real part of  $\mu$ :

$$\lambda_T = \text{Re}(\mu). \quad (9.100)$$

The transverse Lyapunov exponents can be obtained through the method discussed in Section 9.3. The transverse Lyapunov exponents so obtained are

called the average transverse Lyapunov exponents. One can also use the perturbation method to calculate the largest average Lyapunov exponents.

#### 9.4.2 Transverse Lyapunov Exponents in the Presence of Parameter Mismatch

In practice with real physical systems, it is not possible to achieve chaos synchronization without any parameter mismatch. Therefore, it is important to discuss the method of calculating the transverse Lyapunov exponents when the system parameters are mismatched. Instead of using (9.97) and (9.98), we use another set of equations, in which  $\mathbf{g} \neq \mathbf{f}$ , to describe the synchronization when the parameters of the transmitter and the receiver are not perfectly matched:

$$\frac{d\mathbf{x}}{dt} = \mathbf{f}(\mathbf{x}), \quad (9.101)$$

$$\frac{d\mathbf{y}}{dt} = \mathbf{g}(\mathbf{y}) + \alpha \mathbf{D}(\mathbf{x}) - \alpha \mathbf{D}(\mathbf{y}). \quad (9.102)$$

In this case, because the function describing the dynamics of the transmitter is not the same as that describing the dynamics of the receiver, the stability of synchronization is no longer described by the deviation between the transmitter trace and the receiver trace in the coupled phase space. A new concept has to be invented.

We propose the following concept to deal with this situation. Instead of considering the stability of synchronization as the deviation between the transmitter dynamics and the receiver dynamics, we consider the synchronization stability as the deviation between the receiver trace and its nearby traces, using the receiver trace attracted by the transmitter trace in their phase space of the synchronized dynamics as the reference. Therefore, the deviation vector,  $\mathbf{e}(t)$ , is defined in another manner as

$$\mathbf{e}(t) = \mathbf{y}(t) - \mathbf{y}_0(t), \quad (9.103)$$

where  $\mathbf{y}_0(t)$  is the original trace of the receiver synchronized to the transmitter, and  $\mathbf{y}(t)$  is the perturbed trace of the receiver. Therefore, the proposed concept can be quantified to describe the synchronization stability in the presence of parameter mismatch:

$$\frac{d\mathbf{e}}{dt} = \left[ \frac{\partial \mathbf{g}}{\partial \mathbf{y}}(\mathbf{y}_0) - \alpha \frac{\partial \mathbf{D}}{\partial \mathbf{y}}(\mathbf{y}_0) \right] \cdot \mathbf{e}. \quad (9.104)$$

If the function  $\mathbf{g}(\mathbf{y})$  is replaced by the function  $\mathbf{f}(\mathbf{y})$ , this equation is identical to (9.99).

We can use the same procedure described in Subsection 9.3.1 to implement this concept to find the transverse Lyapunov exponents. Alternatively, we can generate a small perturbation in the numerical program on the receiver trace

and then calculate the time evolution of the perturbation. However, we can only obtain the largest transverse Lyapunov exponent from the latter method, which is actually adequate for the stability analysis.

The concept proposed here for analyzing the synchronization stability when the system parameters are mismatched can be considered as a special case of the generalized chaos synchronization proposed by Kocarev and Parlitz [24].

### 9.4.3 Evaluation of the Quality of Synchronization

The simplest and most intuitive method to quantitatively measure the quality of synchronization is to calculate the difference between the traces of the transmitter output and the receiver output as  $\mathbf{e}(t) = \mathbf{y}(t) - \mathbf{x}(t)$ . For the practical purpose of chaotic communications, this synchronization error is normalized to the size of its chaotic attractor. Although there has not been a standard definition of synchronization error, a common one is defined as the following,

$$\zeta = \frac{\langle |X(t) - Y(t)| \rangle}{\langle |X(t)| \rangle}. \quad (9.105)$$

When the synchronization error  $\zeta$  is small, the quality of synchronization is high. Due to its simplicity, this direct measurement of the quality of synchronization is widely used in the numerical simulation of chaos synchronization systems.

In an experiment, however, the nonsimultaneous digitization of experimental data does not allow such direct and precise comparison of the transmitter and receiver outputs to provide a convincing result. A measurement method that is not very sensitive to the digitization error is then more desirable. A common concept known as correlation coefficient is thus usually used for estimating the quality of synchronization of real systems. The correlation coefficient is defined as the following [15],

$$\rho = \frac{\langle [X(t) - \langle X(t) \rangle][Y(t) - \langle Y(t) \rangle] \rangle}{\langle |X(t) - \langle X(t) \rangle|^2 \rangle^{1/2} \langle |Y(t) - \langle Y(t) \rangle|^2 \rangle^{1/2}}, \quad (9.106)$$

where  $X(t)$  and  $Y(t)$  are the outputs of the transmitter and the receiver, respectively, and  $\langle \cdot \rangle$  denotes the time average. The correlation coefficient is bounded as  $-1 \leq \rho \leq 1$ . A larger value for  $|\rho|$  means a higher quality of synchronization. Instead of quantifying the quality of synchronization using the synchronization error, this correlation coefficient measures the similarity of the two attractors.

### 9.4.4 Example: Synchronization of Optically Injected Semiconductor Lasers

We now use a single-mode semiconductor laser subject to optical injection as an example to demonstrate the analysis of the robustness and the quality

of the chaos synchronization. Detailed discussions of the chaos synchronization of this system can be found in Subsection 10.4.1 of Chapter 10, and the configuration can be found in Figure 10.15. Here we concentrate on the mathematical analysis of the robustness and quality of synchronization.

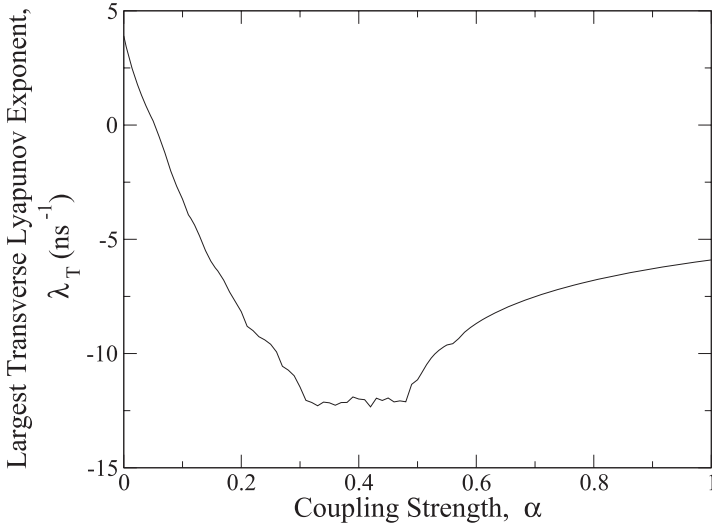


**Fig. 9.6.** Largest global transverse Lyapunov exponent of chaos synchronization as a function of the coupling strength. The chaotic state is generated at  $\xi = 0.03$  and  $f = 0$  GHz. (Reprinted with permission from [22], ©2000 IEEE.)

The dynamics of a semiconductor laser subject to the injection of an optical field is mathematically modeled by the following coupled equations [11],

$$\frac{dA^T}{dt} = -\frac{\gamma_c^T}{2}A + i(\omega_0^T - \omega_c^T)A^T + \frac{\Gamma}{2}(1 - ib^T)gA^T + \eta A_i \exp(-i\Omega t), \quad (9.107)$$

$$\frac{dN^T}{dt} = \frac{J}{ed} - \gamma_s N^T - \frac{2\epsilon_0 n^2}{\hbar\omega_0} g|A^T|^2, \quad (9.108)$$

as is expressed in (9.46) and (9.47). The superscript T labels the variables of the transmitter. The receiver, driven by the transmitted signal  $\alpha A^T(t) + A_i \exp(-i\Omega t + \theta)$  with  $A_i \exp(-i\Omega t + \theta)$  being the optical injection signal, is modeled by the following equations,

$$\frac{dA^R}{dt} = -\frac{\gamma_c^R}{2}A^R + i(\omega_0^T - \omega_c^T + \Delta\omega_c)A^R + \frac{\Gamma}{2}(1 - ib^R)g^R A^R$$

$$+\eta A_i \exp(i\Omega t + i\theta) + \alpha\eta(A^T - A^R), \quad (9.109)$$

$$\frac{dN^R}{dt} = \frac{J^R}{ed} - \gamma_s^R N^R - \frac{2\epsilon_0 n^2}{\hbar\omega_0^T} g^R |A^R|^2, \quad (9.110)$$

where the superscript R labels the variables of the receiver,  $\omega_c$  is the longitudinal mode frequency of the cold laser cavity,  $\Delta\omega_c = \omega_c^T - \omega_c^R$  is the difference between the cold-cavity frequencies of the transmitter and the receiver,  $\alpha$  is the coupling strength of the transmitter output to the receiver, and  $\theta$  is the relative optical phase difference [22]. The definitions of all other parameters can be found in Subsection 7.7.4. Based on the synchronization concept proposed by Kocarev and Parlitz [23], the existence of the perfect synchronization solution,  $A^R = A^T$ , requires  $\theta = 0$ ,  $\Delta\omega_c = 0$ , and that the two lasers be identical except that  $\gamma_c^R = \gamma_c^T + 2\eta\alpha$  [22].

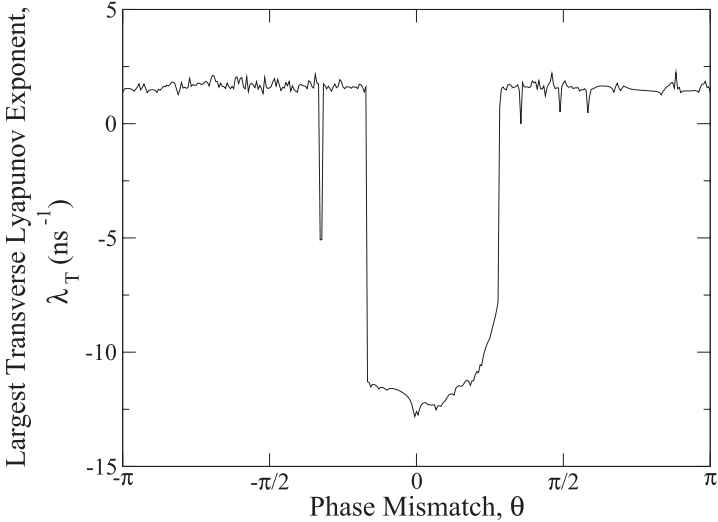


**Fig. 9.7.** Largest global transverse Lyapunov exponent of chaos synchronization as a function of the phase mismatch. The chaotic state is generated at  $\xi = 0.03$  and  $f = 0$  GHz.

The largest global transverse Lyapunov exponent,  $\lambda_T$ , of the coupled system with different coupling strength,  $\alpha$ , is shown in Figure 9.6. The value for each  $\alpha$  is calculated by assigning the matrix  $\mathbf{DF}$  in (9.67) as

$$\mathbf{DF} = \left[ \frac{\partial \mathbf{f}}{\partial \mathbf{x}}(\mathbf{x}) - \alpha \frac{\partial \mathbf{D}}{\partial \mathbf{x}} \right] \quad (9.111)$$

and following the procedure described in Section 9.3.1. It is important to know that  $\lambda_T$  being negative does not guarantee that the local transverse Lyapunov exponent at each segment of the synchronized trace is negative. Therefore, the Lyapunov exponent begins to be negative around  $\alpha = 0.06$ , but robust synchronization will not occur until  $\alpha$  is larger than 0.15 [22]. We can see that an increase in the coupling strength does not necessarily result in an increase in the robustness of synchronization. This phenomenon has been observed in other systems [25]. The most robust synchronization occurs when the value of the coupling strength index is around  $\alpha = 0.4$ . This coupling strength is used when we calculate  $\lambda_T$  for the system operated under the condition of the phase mismatch.

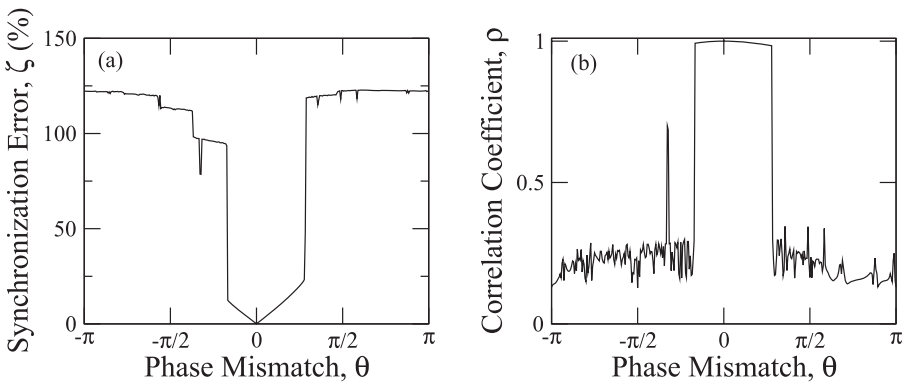


**Fig. 9.8.** Quality of chaos synchronization as a function of the phase mismatch  $\theta$  measured by (a) the synchronization error  $\eta$  and (b) the correlation coefficient  $\rho$ . The chaotic state is generated at  $\xi = 0.03$  and  $f = 0$  GHz.

The effect of the mismatch in many parameters on the robustness and quality of synchronization has been studied for this system [22]. Here we consider only the phase mismatch  $\theta$  for the demonstration of the numerical methods discussed above. The dependence of  $\lambda_T$  on the phase mismatch  $\theta$  is shown in Figure 9.7. The value of  $\lambda_T$  is calculated in this situation by assigning the matrix  $\mathbf{DF}$  in (9.67) as

$$\mathbf{DF} = \left[ \frac{\partial \mathbf{g}}{\partial \mathbf{y}}(\mathbf{y}) - \alpha \frac{\partial \mathbf{D}}{\partial \mathbf{y}} \right] \quad (9.112)$$

and then following the procedure described in Section 9.3.1. As shown, the tolerance of the chaos synchronization to the phase mismatch is in a range of above  $\pi/2$  around  $\theta = 0$ . It is important to check if this characteristic is consistent with the quality of synchronization. The quality measured by  $\zeta$  and

$\rho$  is shown in Figures 9.8a and b, respectively. As is shown, this tolerance can also be observed by examining the quality of the synchronization. A comparison between the curves of  $\lambda_T$ ,  $\zeta$ , and  $\rho$  demonstrates the consistency of these measures.

## 9.5 Chaotic Communications

The standard performance measure of a communication system is the BER for the decoded message as a function of the channel signal-to-noise ratio (SNR) in the transmission channel. The channel SNR is defined as

$$\text{SNR} = \frac{P_m}{\sigma_{\mathbf{X}}^2}, \quad (9.113)$$

where  $P_m$  is the power of the transmitted message, and  $\sigma_{\mathbf{X}}^2$  is the variance of the channel noise  $\mathbf{X}(t)$ . The channel SNR is a function of the channel noise, which is taken to be additive white Gaussian noise, and the bit energy of the transmitted message, which depends on the modulation index of the message.

The BER of the decoded message is a function of the channel noise and the intrinsic noise of the devices in the system, both of which cause synchronization error between the receiver and the transmitter. In a chaotic communication system utilizing chaos synchronization, the synchronization error is caused mainly by the noise, including the channel noise and the transmitter and receiver noise, the message encoding process, and the parameter mismatch between the transmitter and the receiver. The synchronization error is contributed by two forms of error: synchronization deviation, associated with the accuracy of synchronization, and desynchronization bursts, associated with the robustness of synchronization. Synchronization deviation is simply the synchronization error when the system is synchronized, but not perfectly and precisely. Desynchronization bursts are characterized by sudden desynchronization between the transmitter and the receiver. A desynchronization burst can cause a large, abrupt difference between the waveforms of the transmitter and the receiver. Because a system takes some finite time to resynchronize after a desynchronization burst, the bits that follow a desynchronization burst within the resynchronization time are destroyed.

### 9.5.1 Numerical Algorithm for Treating Channel Noise

In the example of simulating the laser dynamics, only the intrinsic noise of the semiconductor laser system is considered. To extend the numerical analysis to the system performance, the numerical method for treating white Gaussian channel noise is necessary and nontrivial. In order to integrate the channel noise into the dynamics of the receiver, the randomness of the channel noise

has to be considered. As is discussed in the simulation of a stochastic differential equation, it is not correct to calculate the channel signal first and then apply the channel signal as a deterministic function of time to the differential equation that describes the dynamics of the receiver. Besides, the channel signal has to be evaluated before it is injected into the receiver in order to include the linear effect of the channel noise. This requires that the effect of the channel noise on system performance be the same as that in a traditional communication system when the nonlinear effect of the channel noise is not considered. The consistency between the linear and the nonlinear effects of channel noise must be satisfied.

The numerical method discussed here is based on the assumption that the channel signal is directly coupled into the receiver at a constant coupling rate. Based on this assumption, the equation of the receiver can be obtained by adding white Gaussian channel noise in (9.102) as the following,

$$\frac{d\mathbf{y}}{dt} = \mathbf{g}(\mathbf{y}) + \alpha\mathbf{D}(\mathbf{x}) - \alpha\mathbf{D}(\mathbf{y}) + \mathbf{N}(\mathbf{X}(t), \mathbf{y}; \eta), \quad (9.114)$$

where  $\mathbf{N}(\cdot)$  is a general function regarding the effect of channel noise on the receiver,  $\eta$  is the coupling rate, and  $\mathbf{X}(t) = (X_1(t), \dots, X_k(t))$  is a generalized  $k$ -dimensional white Gaussian channel noise. Each component of  $\mathbf{X}(t)$  can be expressed as

$$X_i(t) = \sqrt{\frac{N_i}{2}} n_i(t), \quad (9.115)$$

where  $N_i/2$  is the power spectral density of  $X_i(t)$ , and  $n_i(t)$  is a normalized white Gaussian variable with a zero mean, which satisfies (9.2) and (9.3). The variance of  $X_i(t)$  is indicated by  $\sigma_i^2$ . Because all of  $X_i(t)$  are independent of each other, the variance  $\sigma_X^2$  of the entire channel noise  $\mathbf{X}(t)$  with  $\{\sigma_i^2, i = 1, \dots, k\}$  has the following relationship,

$$\sigma_X^2 = \sum_{i=1}^k \sigma_i^2, \quad (9.116)$$

and the power spectral density  $N_X/2$  of  $\mathbf{X}(t)$  with  $\{N_i/2, i = 1, \dots, k\}$  has the following relationship,

$$\frac{N_X}{2} = \sum_{i=1}^k \frac{N_i}{2}. \quad (9.117)$$

Because the dynamics of the transmitter is not affected by channel noise, it is not important in this discussion. Therefore, we only focus on the dynamics of the receiver when the white Gaussian channel noise is considered.

In order to simplify the simulation of stochastic differential equations as is discussed in Subsection 9.2.3, it is preferred that  $\mathbf{N}(\mathbf{X}(t), \mathbf{y}; \eta)$  is not a function of  $\mathbf{y}$ . Thus, the dynamical variables of the receiver should be chosen so that  $\mathbf{N}(\mathbf{X}(t), \mathbf{y}; \eta) = C\eta\mathbf{X}(t)$ , where  $C$  is a constant generated from the

choice of  $\mathbf{y}$ . When this objective is accomplished, each dynamical variable of the receiver is governed by the equation expressed as:

$$\frac{dy_i}{dt} = g_i(\mathbf{y}) + \alpha D_i(\mathbf{x}) - \alpha D_i(\mathbf{y}) + C\eta\sqrt{\frac{N_i}{2}}n_i(t). \quad (9.118)$$

Therefore, the dynamics of the receiver affected by the white Gaussian channel noise can be simulated by following the discussion in Section 9.2 once the value of  $N_i/2$  is known. This equation calculates the nonlinear effect of channel noise on the quality of synchronization and thus message decoding.

However, the channel noise has to be evaluated before it is injected into the receiver because its linear effect has to match that in the traditional communication systems. To generate  $\mathbf{X}(t)$ , its components  $X_i(t)$  are paired and generated through the Box–Muller method [26] as

$$X_{2j-1} = \sqrt{-2\sigma_{2j-1}^2 \ln a_j} \cdot \cos(2\pi b_j), \quad (9.119)$$

$$X_{2j} = \sqrt{-2\sigma_{2j}^2 \ln a_j} \cdot \sin(2\pi b_j), \quad (9.120)$$

where  $j = 1, \dots, [k/2]_{\text{int}}$  with  $[.]_{\text{int}}$  defined as the nearest integer smaller than the value in the bracket, and the pair of  $a_j$  and  $b_j$  are independent random variables evenly distributed in the interval  $(0, 1]$ . The  $a_j$  and  $b_j$  variables for a given  $j$  value are independent of each other, and each pair is also independent of other pairs of different  $j$  values. If the dimension  $k$  of  $\mathbf{X}(t)$  is an odd number, the last unpaired  $X_k(t)$  can be generated by (9.119) with  $2j - 1 = k$ . This evaluation calculates the linear effect of channel noise on message decoding.

It is important to ensure that the nonlinear effect of the channel noise is consistent to the linear effect. Because the nonlinear effect of the channel noise on the dynamics of the receiver is simulated by knowing the value of  $N_i/2$  and the linear effect of the channel noise is evaluated by knowing the value of  $\sigma_i^2$ , a connection between  $N_i/2$  and  $\sigma_i^2$  has to be established. The consistent connection is built based on the twofold effect of this channel noise on the system performance in communication: When the nonlinear effect of the channel noise on the dynamics of the receiver is considered, the receiver will provide natural filtering on the bandwidth of the channel noise. In this situation, the bandwidth of the channel noise does not have to be predefined. When the effect of the channel noise on the dynamics of the receiver is not considered, the effective bandwidth of the channel noise is defined by the bandwidth of the encoding signal. This assumption is the same as the one widely used in a traditional communication system.

Based on this fact, the relationship between  $\sigma_i^2$  and  $N_i/2$  can be established as the following,

$$\begin{aligned} \sigma_i^2 &= \frac{N_i}{2}(2W) \\ &= \frac{N_i}{2}(f_m) \end{aligned}$$

$$= \frac{N_i}{2T_b}, \quad (9.121)$$

where  $W$  is the resolving power and is equal to the half bit rate, and the bit rate  $f_m$  is equal to  $1/T_b$  with  $T_b$  being the bit duration. Thus, the SNR defined in (9.113) can be expressed as

$$\begin{aligned} \text{SNR} &= \frac{P_m}{\sigma_x^2} \\ &= \frac{E_b/T_b}{\sum_{i=1}^k \sigma_i^2} \\ &= \frac{E_b}{\sum_{i=1}^k N_i/2}, \end{aligned} \quad (9.122)$$

where  $E_b$  is the energy per bit. Therefore, once we choose the values of  $E_b$ ,  $T_b$  (or  $f_m$ ), and SNR, the channel noise as a time series can be evaluated by knowing the variance  $\{\sigma_i^2; i = 1, \dots, k\}$ , and the effect of the channel noise on the dynamics of the receiver can be simulated by knowing the values of  $\{N_i; i = 1, \dots, k\}$  and  $\eta$ .

### 9.5.2 Example: Chaotic Optical Communication Using Optically Injected Semiconductor Lasers

Here we use the optical injection system as an example to show the BER as a function of SNR obtained by this method [14]. The rate equation describing the dynamics of the transmitter is given by (9.107) and (9.108), which is not our main interest in this subsection. The rate equation of the receiver after receiving the channel signal including the white Gaussian channel noise is described as the following,

$$\begin{aligned} \frac{dA^R}{dt} &= -\frac{\gamma_c}{2} A^R + i(\omega_0^T - \omega_c^T) A^R + \frac{\Gamma}{2}(1 - ib^R) g A^R + F_{sp}^R \\ &\quad + [1 + m(t)] \eta A_i \exp(-i\Omega t) + \eta \alpha A^T(t) - \eta \alpha A^R(t) + \eta X(t) \end{aligned} \quad (9.123)$$

$$\frac{dN^R}{dt} = \frac{J}{ed} - \gamma_s N^R - \frac{2\epsilon_0 n^2}{\hbar\omega_0} g |A^R|^2, \quad (9.124)$$

where  $m(t)$  is the message and  $X(t)$  is the optical white Gaussian channel noise. In this system,  $X(t)$  is a complex noise term that can be considered as a two-dimensional white Gaussian variable  $X(t) = (X_r(t), X_i(t)) \equiv (X_1(t), X_2(t))$ , where  $X_r(t)$  is the real part and  $X_i(t)$  is the imaginary part of  $X(t)$ . The encoding message  $m(t)$  used in the simulation has non-return-to-zero (NRZ) random digital bits “1” and “0”, with the amplitude of “1” indicated by  $m(t) = \varepsilon$  and that of “0” as  $m(t) = 0$ . The strength of the message can be varied by adjusting the parameter  $\varepsilon$ . The condition of perfect parameter matching is assumed.

As is discussed in Subsection 9.2.4,  $A^R$  is a complex field, which is a two-dimensional variable. In order to ensure that the channel noise term  $\mathbf{N}(\mathbf{X}(t), \mathbf{y}; \eta)$  in (9.114) is decomposed into the form in (9.118), the complex field  $A^R$  is decomposed into its real and imaginary parts as  $A^R = |A_0|(a'^R + ia''^R)$ . Together with  $\tilde{n}^R$  defined by  $N^R = N_0(1 + \tilde{n}^R)$ , the coupled equations (9.123) and (9.124) are recast into the following form,

$$\begin{aligned} \frac{da'^R}{dt} &= \frac{1}{2} \left\{ \frac{\gamma_c \gamma_n}{\gamma_s \tilde{J}} \tilde{n}^R - \gamma_p [(a'^R)^2 + (a''^R)^2 - 1] \right\} (a'^R + ba''^R) \\ &\quad + [1 + m(t)] \xi \gamma_c \cos(2\pi f t) + \frac{F_r}{|A_0|} \\ &\quad + \alpha \eta a'^T - \alpha \eta a'^R + \eta \frac{X_1(t)}{|A_0|}, \end{aligned} \quad (9.125)$$

$$\begin{aligned} \frac{da''^R}{dt} &= \frac{1}{2} \left\{ \frac{\gamma_c \gamma_n}{\gamma_s \tilde{J}} \tilde{n}^R - \gamma_p [(a'^R)^2 + (a''^R)^2 - 1] \right\} (-ba'^R + a''^R) \\ &\quad - [1 + m(t)] \xi \gamma_c \sin(2\pi f t) + \frac{F_i}{|A_0|} \\ &\quad + \alpha \eta a''^T - \alpha \eta a''^R + \eta \frac{X_2(t)}{|A_0|}, \end{aligned} \quad (9.126)$$

$$\begin{aligned} \frac{d\tilde{n}^R}{dt} &= -\gamma_s \tilde{n}^R - \gamma_n \tilde{n}^R [(a'^R)^2 + (a''^R)^2] - \gamma_s \tilde{J} [(a'^R)^2 + (a''^R)^2 - 1] \\ &\quad + \frac{\gamma_s \gamma_p}{\gamma_c} \tilde{J} [(a'^R)^2 + (a''^R)^2 - 1] [(a'^R)^2 + (a''^R)^2]. \end{aligned} \quad (9.127)$$

As the result, the channel noise in (9.125) and (9.126) above have the same form as that in (9.118).

Because  $X_1(t)$  and  $X_2(t)$  have the same magnitude,  $\sigma_X^2 = 2\sigma_1^2 = 2\sigma_2^2$  and  $N_X = 2N_1 = 2N_2$ . Thus, the SNR can be expressed as

$$\begin{aligned} \text{SNR} &= \frac{E_b/T_b}{2\sigma_1^2} = \frac{E_b}{N_1} \\ &= \frac{E_b/T_b}{2\sigma_2^2} = \frac{E_b}{N_2}. \end{aligned} \quad (9.128)$$

Once the values of  $\varepsilon$ ,  $T_b$  (or  $f_m$ ), and SNR are determined, the values of  $E_b$ ,  $\sigma_1^2$ ,  $\sigma_2^2$ ,  $N_1$ , and  $N_2$  can be obtained through (9.128). Therefore, the dynamics of the receiver can be numerically simulated through (9.125)–(9.127) with the white Gaussian channel noise evaluated through (9.119) and (9.120).

To examine this method by using this example, it is important to know that the nonlinear effect of channel noise does not contribute to the BER of this laser system when the term  $\eta X(t)$  in (9.126) is set to zero. This assumes that the channel noise does not inject into the receiver laser; thus the quality of synchronization is not affected by the channel noise. Therefore, when  $\eta X(t) = 0$ , the performance of this system can be directly compared to that

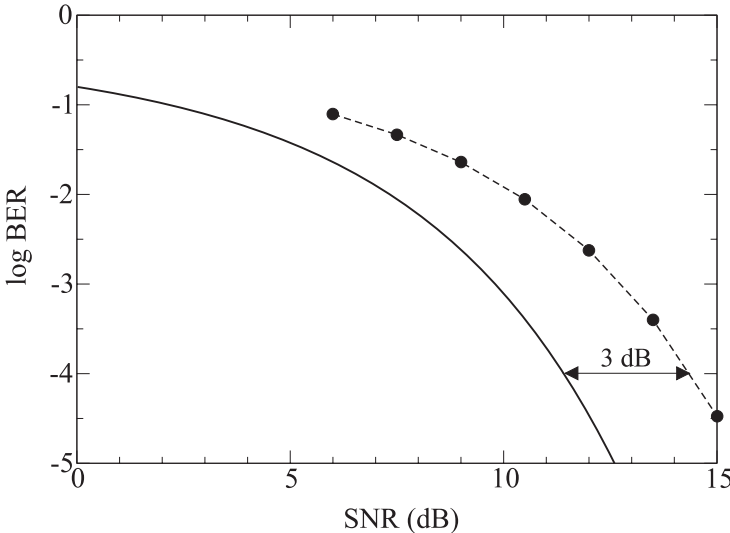


**Fig. 9.9.** Comparison between the BER as a function of SNR for BPSK and that for the optically injected semiconductor laser system when the channel noise is not injected into the receiver. The solid curve indicates the BER of BPSK, and the dashed curve marked with solid circles indicates the BER of the optical injection system when the nonlinear effect of the channel noise on the receiver is turned off numerically. The transmitter is operated at  $\xi = 0.03$  and  $f = 0$  GHz to generate the chaotic waveform as the message carrier. Perfect chaos synchronization is assumed.

of a traditional communication system. As an examination of this method, the BER of this laser system with  $\eta X(t) = 0$  is compared to that of a traditional binary phase shift keying (BPSK) system. In Figure 9.9, the BER as a function of the SNR for BPSK is shown as the solid curve, and that for the optical injection system with  $\eta X(t) = 0$  is shown as the dashed curve marked by solid circles. The solid circles show the value of BER obtained through the numerical simulation using (9.125)–(9.127), and the dashed curve just provides the visual aid. Because the encoding message used in BPSK has NRZ random digital binary bits “0” and “1” with  $m(t) = -\varepsilon/2$  as the bit “0” and  $m(t) = \varepsilon/2$  as the bit “1” [15], the  $E_b$  of BPSK is only half that of the encoding method used in this optical injection system. Therefore, a 3-dB difference in the SNR for the same BER should be expected. This 3-dB difference is marked in Figure 9.9.

The BER as a function of the SNR from the numerical simulation of (9.125)–(9.127) with nonzero  $\eta X(t)$  is shown in Figure 9.10 [14]. The transmitter is operated at  $\xi = 0.03$  and  $f = 0$  GHz to generate the chaotic waveform as the message carrier. The intrinsic laser noise of the transmitter and that of the receiver are both ignored in this simulation to see clearly the effect of the channel noise. Each curve is obtained by fixing the message amplitude while

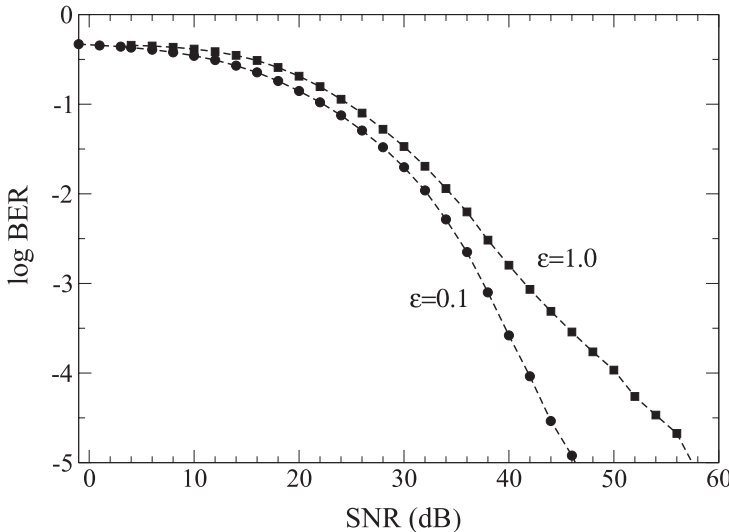


**Fig. 9.10.** BER as a function of SNR(dB) for the optically injected semiconductor laser system when the system performs chaos synchronization. The dashed curve marked with solid circles is obtained when  $\varepsilon = 0.1$ , and the dashed curve marked with solid squares is obtained when  $\varepsilon = 1.0$ . The transmitter is operated at  $\xi = 0.03$  and  $f = 0$  GHz to generate the chaotic waveform as the message carrier. (Reprinted with permission from [14], ©2002 IEEE.)

changing the strength of the channel noise. The dashed curve marked with solid circles is obtained when  $\varepsilon = 0.1$ , and the dashed curve marked with solid squares is obtained when  $\varepsilon = 1.0$ . As is shown, the performance analysis of the system with the same SNR but different  $\varepsilon$ , or equivalently different  $E_b$ , results in different values of the BER. Because the channel noise increases with  $E_b$  for a given SNR, this dependence of the BER on  $E_b$  at a fixed SNR demonstrates the nonlinear effect of the channel noise on the system performance.

## 9.6 Conclusions

This chapter provides a detailed discussion of the most important numerical tools needed in the analysis of chaotic systems performing chaos synchronization and chaotic communications. Basic concepts, theoretical framework, and computer algorithms are reviewed. The subjects covered include the concepts and numerical simulations of stochastic nonlinear systems, the complexity of a chaotic attractor measured by Lyapunov exponents and correlation dimension, the robustness of synchronization measured by the transverse Lyapunov exponents in parameter-matched systems and parameter-mismatched systems, the quality of synchronization measured by the correlation coefficient and the synchronization error, and the treatment of channel noise for quantifying the

performance of a chaotic communication system. Optically injected single-mode semiconductor lasers are used as examples to demonstrate the use of these numerical tools.

The discussion on a dynamical system described by a stochastic differential equation shows that the integral of a stochastic term in the equation is very different from that of a deterministic term. When the first order of the integral is considered, the integral of a stochastic term is proportional to the square root of the infinitesimal time interval. In comparison, that of the deterministic term is proportional to the infinitesimal time interval. There are two types of integrals for solving a stochastic differential equation, namely, the Ito integral and the Stratonovich integral. Which method has to be used depends on the characteristics of the noise. It is revealed that the calculation in the Stratonovich sense follows the rules of the Riemann–Stieltjes integral, but the white noise term in the equation is no longer white noise. The calculation in terms of the Ito sense assures that the white noise treated in the integral is still white noise, but the calculation does not follow the rules of the Riemann–Stieltjes integral. A connection between these two methods is given in this chapter.

Two quantitative measures, namely, the Lyapunov exponents and the correlation dimension, for a chaotic attractor are discussed. The Lyapunov exponents measure the sensitivity of a chaotic system to initial conditions and perturbations. The correlation dimension increases with the complexity of a chaotic attractor. Numerical methods for calculating these parameters are outlined. When the dimension of a chaotic attractor is very high, the calculation of the largest Lyapunov exponent is preferred because it greatly simplifies the numerical computation.

The robustness of synchronization is measured by the transverse Lyapunov exponents. Either the whole set of transverse Lyapunov exponents or the largest transverse Lyapunov exponent can be used to measure the robustness. Usually only the largest transverse Lyapunov exponent is important. Thus, the calculation of the largest transverse Lyapunov exponent is preferred when the system is very complex. Because perfect parameter matching between a transmitter and a receiver is generally not possible in a real system, a new concept of robustness of synchronization is introduced for a system with parameter mismatch. For a perfectly parameter-matched synchronization system, the robustness of synchronization is measured between the attractors of the transmitter and the receiver. However, when the parameters of the system are not perfectly matched, this comparison between the transmitter and the receiver is impossible. Therefore, the comparison is made between the unperturbed and perturbed receiver attractors when synchronization is achieved. For the examination of the quality of synchronization, the correlation coefficient and the synchronization error obtained by the direct comparison between the transmitter and the receiver waveforms are used. Because it is very difficult to obtain both chaotic waveforms with exactly simultaneous digitization when they are measured in experiment, a direct comparison between the

transmitter and the receiver waveforms is usually not accurate. Therefore, the measurement using the correlation coefficient is preferred for the experimental data because it is less sensitive to digitization timing errors.

The performance of a communication system is commonly measured by the BER as a function of SNR. In addition to the noise in the transmitter and the receiver, the noise of the communication channel has to be considered in evaluating the BER and SNR of the system. The white channel noise in a synchronized chaotic communication system interacts nonlinearly with the nonlinear system. For example, the channel noise can cause the receiver to lose synchronization with the transmitter, thus resulting in a large bit error. Therefore, both the linear effect of the channel noise as its role in conventional communication systems and the nonlinear effects of the channel noise have to be considered in a chaotic communication system. An approach to integrating the linear and nonlinear effects of the channel noise into the system consistently is addressed.

## Acknowledgments

This work was supported by the U.S. Army Research Office under MURI grant DAAG55-98-1-0269.

## References

1. C. C. Chen and K. Yao, Stochastic-calculus-based numerical evaluation and performance analysis of chaotic communication systems, *IEEE Trans. Circuits Syst. I*, vol. 47, pp. 1663–1672, 2000.
2. T. B. Simpson and J. M. Liu, Spontaneous emission, nonlinear optical coupling, and noise in laser diodes, *Opt. Commun.*, vol. 112, pp. 43–47, 1994.
3. J. M. Liu, C. Chang, T. B. Simpson, Amplitude noise enhancement caused by nonlinear interaction of spontaneous emission field in laser diodes, *Opt. Commun.*, vol. 120, pp. 282–286, 1995.
4. R. Mannella and V. Pallesche, Fast and precise algorithm for computer simulation of stochastic differential equations, *Phys. Rev. A*, vol. 40, pp. 3381–3386, 1989.
5. R. L. Honeycutt, Stochastic Runge–Kutta algorithms I. White noise, *Phys. Rev. A*, vol. 45, pp. 600–603, 1992.
6. E. Helfang, Numerical integration of stochastic differential equations, *The Bell Syst. Tech. J.*, vol. 58, pp. 2289–2298, 1979.
7. R. F. Fox, I. R. Gatland, R. Roy, and G. Vemuri, Fast, accurate algorithm for numerical simulation of exponentially corrected colored noise, *Phys. Rev. A*, vol. 38, pp. 5938–5940, 1988.
8. C. W. Gardiner, *Handbook of Stochastic Methods for Physics, Chemistry, and the Nature Sciences*, 2nd ed. (Springer, New York, 2001).

9. S. Cyganowski, P. Koleden, and J. Ombach, *From Elementary Probability to Stochastic Differential Equations with MAPLE* (Springer, New York, 2001).
10. V. S. Anishchenko, V. V. Astakhov, A. B. Neiman, T. E. Vadivasova, and L. Schimansky-Geier, *Nonlinear Dynamics of Chaotic and Stochastic Systems* (Springer, New York, 2001).
11. J. M. Liu, H. F. Chen, X. J. Meng, and T. B. Simpson, Modulation bandwidth, noise, and stability of a semiconductor laser subject to strong injection locking, *IEEE Photon. Techno. Lett.*, vol. 9, pp. 1325–1327, 1997.
12. T. B. Simpson, J. M. Liu, A. Gavrielides, V. Kovanis, and P. M. Alsing, Period-doubling route to chaos in a semiconductor laser subject to optical injection, *Appl. Phys. Lett.*, vol. 64, pp. 3539–3541, 1994.
13. S. K. Hwang, J. B. Gao, and J. M. Liu, Noise-induced chaos in an optically injected semiconductor laser model, *Phys. Rev. E*, vol. 61, pp. 5162–5170, 2000.
14. S. Tang, H. F. Chen, S. K. Hwang and J. M. Liu, Message encoding and decoding through chaos modulation in chaotic optical communications, *IEEE Trans. on Circuits Syst. I*, vol. 49, pp. 163–169, 2002.
15. S. Haykin, *Communication Systems*, 3rd ed. (John Wiley & Sons, New York, 1994).
16. H. D. I. Abarbanel, R. Brown, and M. B. Kennel, Lyapunov exponents in chaotic systems: their importance and their evaluation using observed data, *Int. J. of Modern Phys.*, vol. 5, pp. 1347–1375, 1991.
17. R. Brown, P. Bryant, and H. D. I. Abarbanel, Computing the Lyapunov spectrum of a dynamical system from an observed time series, *Phys. Rev. A*, vol. 43, pp. 2787–2806, 1991.
18. J. B. Gao, S. K. Hwang, and J. M. Liu, Effects of intrinsic spontaneous-emission noise on the nonlinear dynamics of an optically injected semiconductor laser, *Phys. Rev. A*, vol. 59, pp. 1582–1585, 1999.
19. P. Grassberger and I. Procaccia, Characterization of strange attractors, *Phys. Rev. Lett.*, vol. 50, pp. 346–349, 1983.
20. J. Theiler, Estimating fractal dimension, *J. Opt. Soc. Am. A*, vol. 7, pp. 1055–1073, 1990.
21. E. V. Grigorieva, H. Haken, and S. A. Kaschenko, Theory of quasiperiodicity in model of lasers with delayed optoelectronic feedback, *Opt. Commun.*, vol. 165, pp. 279–292, 1999.
22. H. F. Chen and J. M. Liu, Open-loop chaotic synchronization of injection-locked semiconductor lasers with gigahertz range modulation, *IEEE J. Quantum Electron.*, vol. 36, pp. 27–34, 2000.
23. L. Kocarev and U. Parlitz, General approach for chaotic synchronization with applications to communication, *Phys. Rev. Lett.*, vol. 74, pp. 5028–5031, 1995.
24. L. Kocarev and U. Parlitz, Generalized synchronization, predictability, and equivalence of unidirectionally coupled dynamical systems, *Phys. Rev. Lett.*, vol. 76, pp. 1816–1911, 1996.
25. L. M. Pecora, T. L. Carroll, G. A. Johnson, D. J. Mar, and J. F. Heagy, Fundamentals of synchronization in chaotic systems, concepts, and applications, *Chaos*, vol. 7, pp. 520–543, 1997.
26. D. E. Knuth, *Seminumerical Algorithms*, vol. 2 of *The Art of Computer Programming*, 3rd ed. (Addison-Wesley, Reading, MA), p. 122, 1997.